Anther Dehiscence Is Regulated By Gibberellic Acid In Yellow Lupine (Lupinus Luteus L.)

Katarzyna Marciniak (marciniak@umk.pl)

Nicolaus Copernicus University, Faculty of Biological and Veterinary Sciences, Chair of Plant Physiology and Biotechnology, Lwowska 1 St, 87-100 Toruń, Poland https://orcid.org/0000-0002-8681-9935

Krzysztof Przedniczek

Nicolaus Copernicus University in Torun: Uniwersytet Mikolaja Kopernika w Toruniu

Research article

Keywords: Anther dehiscence, gibberellins, endothecium, secondary thickening, septum/stomium rupture, degeneration via PCD, yellow lupine, legumes

Posted Date: January 14th, 2021

DOI: https://doi.org/10.21203/rs.3.rs-143812/v1

Abstract

Background:

Anther dehiscence resulting in the release of pollen grains is tightly regulated in spatio-temporal manner by various factors. In yellow lupine (*Lupinus luteus* L.), the species which shows cleistogamy, the anthers split before the flowers open but the course and regulation of this process is unknown. Specific control of the anther development takes place with the participation of hormonal pathways, the wide action of which ensures reproductive success. In our previous research we have shown that the lowest transcript level of *LlDELLA1*, a main repressor of gibberellin (GA) signaling, in flower and early pod development occurs about the time of anther opening; therefore the main purpose of this study was to precisely investigate the gibberellic acid (GA_3)-dependent regulation of anther dehiscence program in yellow lupine.

Results:

In this paper we showed the specific changes in the yellow lupine anther structure during the dehiscence and identified several genes widely-associated with this process, including deposition of lignocellulosic secondary thickening in the endothecium, enzymatic breakdown of cell walls at the septum/stomium and cell degeneration via programmed cell death (PCD). The expression profile of genes varied over time with the most intense mRNA accumulation in the phases prior to or about time of anther opening. The transcriptional activity revealed also that these genes are highly co-expressed and regulated in a GA-dependent manner. The cellular and tissue localization of GA_3 exhibited that these molecules are present right before anther opening, mainly in septum cells, near the vascular bundle and in the endothecium, and later they were completely undetectable. The GA_3 localization strongly correlates with the transcriptional activity of genes related with GA biosynthesis and deactivation. The obtained results also suggest that GA_3 controls *LlGAMYB* expression via *LlMIR159*-dependent pathway.

Conclusions:

The presented results show a clear contribution of GA_3 in the control of the extensive anther dehiscence program in yellow lupine. Understanding the processes underlying pollen release at hormonal and molecular level is a significant aspect in controlling fertility in economically important legume crop species and increased attention of breeders.

Background

The critical point of plant reproduction is proper development of stamens and release of viable pollen grains followed by pollination, fertilization and finally fruit/pod setting and development. This is particularly important in crop plants, including legumes, due to the impact on the yield. Knowledge of stamen development is increasing successively, but most information comes from analyzes of male sterile mutants in *Arabidopsis thaliana* and rice (*Oryza sativa*) [1, 2, 3, 4, 5]. Fourteen phases of stamen development have been identified in a model plant *A. thaliana* [1]. During the early phases, the epidermis

and stomium are formed from the L1 layer; the L3 layer is divided into connective and vascular bundle, while the L2 layer gives rise to initial archesporial cells (AC). Then, from AC two cell lines are generated - primary parietal cells (PPC) and primary sporogenous cells (PSC). The PPC differentiate into endothecium, middle layer and tapetum, while the PSC produce the tetrad of haploid microspores as a result of meiosis. In the late phases, the microspores develop into pollen grains, the filament elongates and the anther opens [6, 7]. The fundamental and extensive process that occurs in maturing stamens is anther dehiscence, which in general consists of the following stages: (I) expansion of the endothecium and deposition of wall thickenings in endothecial and connective cells; (II) degeneration of the tapetum and middle layer (stages 7–11); (III) enzymatic opening of the septum between two locules and its progressive degeneration (stages 11–12); (IV) breakage of the stomium formed from modified epidermal cells (stage 12); and finally (V) pollen grains release from the locules during stage 13. Eventually, the anther senescence and is separated from the flower (stages 14a-14c) [1, 2]. Many species, such as *A. thaliana*, tobacco (*Nicotiana tabacum*) and rice, exhibit comparable course of anther dehiscence program [1, 8, 9, 10]. The differentiation and degeneration of the septum (circular cell cluster in *N. tabacum*) and stomium are conserved [8]; however, the developmental differences exist, e.g. in anther structure or types of endothecial thickening [11, 12]. There are many evidences demonstrating crucial role of secondary cell wall thickening in pollen release. It is suggested that this is closely related to the delivery of force to disrupt the stomium cells [2, 4, 11]. The key components of secondary cell walls are lignin, cellulose and hemicelluloses (xylan and glucomannan). Lignin consists of three subunits, namely p-hydroxyphenyl (H), guaiacyl (G) and syringyl (S), while the most important enzyme catalyzing the last step of lignin biosynthesis is cinnamyl alcohol dehydrogenase (CAD) [13]. In *A. thaliana*, two *CAD* genes (*CAD C*, *CAD D*) are identified and mutants of these genes show the absence of lignin in the endothecium leading to anther indehiscence [14]. Among the genes involved in secondary cell wall formation *IRREGULAR XYLEM1/6/8* (*IRX1/6/8*) can be also distinguished [15, 16, 17]. The *IRX1* with alternative name *Cellulose synthase A catalytic subunit 8* (*CesA8*) is required for the synthesis of cellulose [16]; the *IRX6* (synonym *COBRA-like4*, *COBL4*) encodes a member of the COBRA family that is needed for the deposition of cellulose, whereas *IRX8* (synonym *Galacturonosyltransferase12*, *GAUT12*) belongs to the CAZy family of Glycosyl Transferase (GT8) that is involved in the deposition of xylan and lignin in the secondary cell walls [15, 18]. One of the major events in the anther dehiscence is also pectin degradation leading to cell separation which involves enzymes such as polygalacturonases (PGs). QUARTET2 (QRT2), as part of a small family of endo-PGs, has been identified as involved in anther dehiscence process [4, 19]. Many papers have shown that septum and stomium go through a process of degeneration and cell death via developmental programmed cell death (PCD)-related process, as part of the dehiscence program. Furthermore, plant cells undergo PCD usually in response to hormone-mediated signaling pathways [8, 20]. Among genes associated with PCD, in *A. thaliana* the *PROMOTION OF CELL SURVIVAL 1* (*PCS1*) has been recognized as important factor encoding an aspartic protease that acts during reproduction and embryogenesis. Using the transgenic plants that overexpressed *PCS1*, Ge et al. showed that this gene inhibit the individual elements of the PCD pathway in anther [21].

Examination of late-dehiscence mutants revealed that time of anther opening is strictly controlled by various factors, including phytohormones. Usually *A. thaliana* mutants that are defective in phytohormone biosynthesis or perception are male sterile and have anthers that split too late for effective pollination and fertilization [8, 9, 22, 23]. Gibberellins (GAs) play an important role in the control of pollen formation and viability, filament elongation as well as anther dehiscence [5, 24, 25, 26, 27, 28]. Late GA biosynthesis stages are catalyzed by gibberellin 3-oxidases (GA3oxs) responsible for the production of active phytohormone molecules and gibberellin 2-oxidases (GA2oxs) that deactivate GAs. The central factor in the GA signaling pathway is *GAMYB* belonging to the R2R3-MYB subfamily. The results of research on barley (*Hordeum vulgare*) show that overexpressing the *HvGAMYB* results in phenotype with indehiscent anther [29]. Another studies revealed, that *GAMYB* acts in cooperation with microRNA, especially miR159 [30]. These facts indicate that a complex set of interactions is required to coordinate events within the flower leading to anther dehiscence.

The developmental timing of anthers opening influences the type of pollination and the degree of self-pollination in comparison with cross-pollination. This is important for seed production in breeding programs and agriculture. In general, pollen release occurs when flowers are fully open, in *A. thaliana* at flower stage 13 [31]; however, in some plants, including yellow lupine (*Lupinus luteus* L.) a special type of self-pollination in a closed flower (cleistogamy) was found. Yellow lupine is also characterized by the ability to fix atmospheric nitrogen, as well as high protein content in seeds; therefore it is worldwide used as food and feed source. Nevertheless, this legume plant has problem of premature flower abortion [32, 33, 34, 35]. For years, there has been a hypothesis that the reason for excessive flower separation may be incorrect stamen development, and as a consequence insufficient pollination, fertilization, and pod setting, which finally reduces yield. Our earlier study has shown that changing level of *LIDELLA1* mRNA, encoding major repressors of GA signaling, supports the correct flower and pod development [34]. Interestingly, the expression of *LIDELLA1* in the closed-flower bud phase is relatively high and then slightly decreased until the anther opening, while during pollination, fertilization and early pod development the gradual increase of transcript level is observed. This indirectly indicates the involvement of GAs in flower development, including stamens. Therefore, the main aim of this study was to understand the process of GA-modulated late anther development in yellow lupine, which may lead in the future to the control of male fertility, which eliminates the problem of low yielding. We focused on genes and proteins that could be potential markers of developmental changes taking place in yellow lupine anthers. Examination of the expression profile of genes widely associated with the dehiscence program after the application of various compounds (gibberellic acid, GA_3 and paclobutrazol, PAC) in conjunction with GA_3 immunolocalization provides a broad insight into the regulation of the anther development process in yellow lupine. The function of predicted proteins was defined based on the presence of conserved domains, motifs and specific amino acids. The research is complemented by histological analyzes determining changes in the structure of the yellow lupine anther during the process of the extensive dehiscence.

Results

Specific changes of anther structure during dehiscence program of yellow lupine

The individual stages of yellow lupine late anther development (LAD), when dehiscence program takes places, have been selected (Fig. 1A). In the first phase of LAD (1 LAD), which corresponds to *A. thaliana* phase 11, the four separated locules with pollen were distinguished (Fig. 1B). Therefore, the anther is bithecal and tetrasporiangiate. In the center of the yellow lupine anther, connective tissue containing a vascular bundle with septum on both sides (each of them separates the locules) was found. Moreover, the septum cells are characterized by different sizes depending on their location, with a tendency that cells closer to the anther center are much larger. The wall surrounding the anther locules consists of following cell layers: epidermis, endothecium, middle layer, and tapetum. Externally located epidermis is composed of one layer of longitudinally elongated cells. The differentiated epidermal cells form the stomium region adjacent to septum cells. The next layer consists of the transversely elongated endothecial cells with visible secondary cell wall thickening. Additionally, the remains of the tapetum are visible in locules (Fig. 1B). In the 1 LAD phase breakage of the septum from the stomium was also noticed (Fig. 1C). This generates a bilocular anther and further degeneration of the septum cells were evident in the second LAD phase (2 LAD) (corresponding to *A. thaliana* phase 12) (Fig. 1D). It was observed that stomium forms a single cell region, the location of which determines the position of anther opening. The late septum shrinkage and disruption seems to contribute to breaking the stomium, which leads to pollen release (these processes occur simultaneously). Dehiscence process does not affect the central connective cells, which remain joined. Yellow lupine anther opening occurs in 2 LAD phase, which corresponds to phase 13 in *A. thaliana* (Fig. 1E). Following dehiscence the anther senescence (3 LAD, Fig. 1F/G). This phase is characterized by further degeneration and shrinkage of cells, as well as entire anther structure (4 LAD, Fig. 1H/I).

Secondary thickening of endothecial cell walls

In first stage of yellow lupine anther dehiscence program, the endothecium, which partially surrounds the locule, undergoes formation and deposition of secondary thickening (Fig. 2A). The endothecial cell walls have U-shaped thickening. The same occurs in the connective cell walls, but to a much lesser extent. Other anther cells, which create for example epidermis, septum or stomium region, do not undergo thickening, which suggests that secondary thickenings are strictly localized in endothecium.

The expression profile of secondary wall-associated genes (Fig. 2B) with and without GA_3 application in all LAD phases in yellow lupine was established (Fig. 2C). In the first and second LAD phases, a significantly higher expression level of *LICAD* and all *LIIRX* genes was observed compared to the third and fourth LAD phases. In addition, the GA_3 treatment increased the number of lignin/cellulose/xylan biosynthesis gene transcripts, especially in the second LAD phase. It can be concluded that the genes related to secondary thickening of the endothecial cell walls show co-upregulated expression and their

transcriptional activity is associated mainly with changes in the first and second LAD stages of yellow lupine. Additionally, it appears that the level of transcripts of all identified genes is GA dependent.

Breakdown of the septum/stomium cells

Cell separation is an important event that takes place in yellow lupine anther. The dehiscence program involves interruption of the cell wall material between adjacent cells (Fig. 3A). It is likely that in this process endo-PGs and phytohormones are involved. In selected stages of LAD, we examined the transcriptional activity of *QRT2* encoding the marker enzyme involved in rupture the pectin between cells (Fig. 3B). Obtained results indicate that the amount of *LlQRT2* mRNAs is high in the first and second LAD phase where breakdown of the septum/stomium takes place. In the third and fourth LAD phase lower level of transcripts was detected. Interestingly, *LlQRT2* expression is stimulated by GA_3, especially in the second LAD stage.

Degeneration of septum/stomium cells via PCD-related process

The yellow lupine anther septum and stomium go through degeneration process and cell death to facilitate pollen release via GA-dependent PCD-related process (Fig. 3C). To prove this, we specified the expression profile of *LlPCS1* which encodes aspartic protease being anti-cell death component. As expected, GA_3 application decreased the transcriptional activity of *LlPCS1*, especially in the first and fourth stages of LAD (Fig. 3D). This indirectly shows that GA_3 by inhibiting the anti-PCD factor favors this process in yellow lupine anthers.

Cellular and tissue localization of gibberellic acid during yellow lupine anther development

Due to the fact that in previous experiments it turned out that GA_3 regulates the expression of genes associated with both the secondary thickening of endothecial cells and degeneration of cells via enzymatic breakdown and PCD-related process, we have performed cellular and tissue immunolocalization of GA_3 in all selected stages of anther maturation in yellow lupine (Fig. 4). The obtained results showed that the highest accumulation of GA_3 occurs in the first LAD phase before anther opening (Fig. 4A/A'). At the cellular level, the strongest fluorescence signal was noted in the entire cytoplasm of degenerating septum cells at the time of bilocular anther formation (the cells were filled with GA_3). A high level of phytohormone molecules was also observed near the vascular bundle, in the cells of middle layer and endothecium, as well as in the epidermis but to lesser extent. Compared to the first stage, in the second LAD phase, where the stomium cells are disrupted and the pollen chambers are opened, a fluorescence signal indicating GA_3 content was almost imperceptible (Fig. 4B/B'). The sites where GA_3 was found were the cells of progressively degenerating septum, middle layer, and near the vascular bundle. After the anther was opened and mature pollen grains were released (3 LAD stage), no

fluorescence signal was found that would indicate the presence of GA_3 in any cell and tissue (Fig. 4C). When complete cell degeneration and aging of the anther occurred (4 LAD stage), GA_3 signal was also not detected. The lack of cell nuclei is also noticeable, which indicates the rapidly progressing processes of degeneration and death of the entire cells of anther.

GA_3 localization correlates with GA metabolism

The expression profile of *LlGA3ox* involved in the formation of active phytohormone molecules and *LlGA2ox1* responsible for the GA inactivation was determined (Fig. 5) in order to verify whether it correlates with the endogenous GA_3 level. In subsequent stages of LAD, a decrease in the *LlGA3ox* mRNA level was observed (Fig. 5A). In the case of *LlGA2ox1*, the opposite situation was found (Fig. 5B). Furthermore, the use of PAC, which inhibits the early stage of GA biosynthesis, reduced significantly the expression of both studied genes.

GA_3 controls LlGAMYB expression via mir159-dependent pathway during late anther development

In yellow lupine, GA_3 likely participates in the regulation of *LlGAMYB* by controlling the *LlMIR159* expression level. Both *LlGAMYB* and *LlMIR159* transcriptional activity in four selected phases of LAD, as well as after GA_3 and PAC application was examined (Fig. 6). The *LlGAMYB* expression was almost identical with or without GA_3 treatment, but the lack of GA_3 due to PAC application resulted in increased *LlGAMYb* transcripts, especially in first and second LAD stages (Fig. 6A). These results suggest that GA_3 possibly regulates *LlGAMYB* expression but not directly. Due to this fact we examined *LlMIR159* expression profile (Fig. 6B). The GA_3 treatment increases the *LlMIR159* mRNA level, and importantly, PAC application significantly decreases the expression of *LlMIR159*. By analyzing the natural conditions without the application of any compounds, it can be concluded that *LlGAMYB* expression remains at a higher level in the first two stages of LAD and then decreases. This negatively correlates with the transcriptional activity of the *LlMIR159*, which was significantly increased in the second phase of LAD. This is probably the cause of the reduced mRNA content of the *LlGAMYB* in third and fourth LAD stages. The obtained results suggest that *LlGAMYB* is co-expressed with *LlMIR159* in yellow lupine anthers. It also follows that *LlGAMYB* transcript level is potential regulated by miR159 in anther of yellow lupine.

In silico analyses of studied genes

The identification of many genes encoding enzymes connected with anther dehiscence prompted us to perform bioinformatics analyzes. The full-length cDNA sequences identified in yellow lupine, their deduced amino acid sequences, as well as molecular weight, predicted isoelectric point and accession numbers from the NCBI database were presented (Fig. S1a, S2a, S3a, S4a, S5a, S6a, S7a, S8a, S9a). Maximum likelihood phylogenetic trees of different proteins with the highest degrees of similarity/identity to proteins predicted in yellow lupine were constructed (Fig. S1b, S2b, S3b, S4b, S5b, S6b, S7b, S8b, S9b).

In all cases, the yellow lupine proteins showed the closest relationship to proteins derived from legumes, especially narrow-leaf lupine (*L. angustifolius*). To better understand the function of all yellow lupine proteins, conserved domains, motifs and specific amino acids were discovered and localized (Fig. 7A'-F'; Fig. 8A'-C'). The positions of all conserved domains, motifs and amino acids present in yellow lupine were confronted and confirmed on the background of similar proteins occurring in many plant species (Fig. S1c, S2c, S3c, S4c, S5c, S6c, S7c, S8c, S9c). Additionally, the predicted yellow lupine proteins have been assigned a likely function based on that described in other plant species (Table 1). The tertiary structures of yellow lupine proteins were predicted using Robetta service (Fig. 7A-F; Fig. 8A-C). Additionally, the amino acid sequences of yellow lupine were compared with those from other plant species. Both the similarity and the number of identical amino acids are included (Fig. S1d, S2d, S3d, S4d, S5d, S6d, S7d, S8d, S9d). It follows that proteins such as CAD, CesA8, COBL4 or GAUT12 are strictly conserved among the plant kingdom, while the remaining ones (PG/QRT2, PCS1, GA3ox, GA2ox, GAMYB) show a great affinity among closely related species, but much less identity/similarity to such as, for example, *A. thaliana*.

Table 1

Predicted function of conserved domains, motifs and specific amino acids in yellow lupine proteins [LlCAD (Cinnamyl Alcohol Dehydrogenase); LlCesA8/LlIRX1 (Cellulose synthase A catalytic subunit 8/IRREGULAR XYLEM1); LlCOBL4/IRX6 (COBRA-like4); LlGAUT12/LlIRX8 (GAlactUronosylTransferase12); LlPG/LlQRT2 (Polygalacturonase/ QUARTET2); LlPCS1 (PROMOTION OF CELL SURVIVAL1); LlGA3ox (Gibberellin 3-oxidase); LlGA2ox1 (Gibberellin 2-oxidase1); LlGAMYB)] based on data published in other plant species.

Protein	Identified conserved domains/motifs/specific amino acids	Predicted functions
LlCAD	Alcohol dehydrogenase GroES-like domain	Catalytic domain with GroES-like structure [38]
	Zinc-binding dehydrogenase domain	Catalytic activity, zinc ion binding [38]
	Zn-1 (GHExVGxVxxxGxxV) and Zn-2 (GxxVGxGxxxxxCxxCxxCxxxxxxxC) binding motifs	Zn-1 catalytic centre and Zn-2 binding site [39]
	Three amino acids C, H, C	Define places of catalytic Zn action [40]
	Four C residues	Structural Zn ligation (Zn-2 structural motif) [40]
	G residues (GxGGxG) (so-called Rossmann fold) represent NADPH co-substrate-binding motif	G residues for substrate specificity [40]
	S 212	Specific NADP(H) binding residue [40]
	Many conserved residues: S, Q, L, M, W, V, P, L, F, I	Determine substrate ligation [38]
LlCesA8/ LlIRX1	N-terminal region inclusive of a Zn-binding RING motif with a strictly conserved CxxC sequence motif beginning amino acids: $CxxCx_{12}FxACxxCxxPxCxxCxExxxxxDxxxCxxC$	Protein-protein interactions in the CesA complex [41, 42, 43]
	Hypervariable region (VR1) of 117 aa, rich in acidic aa	This region is more conserved than was previously thought. The contribution of this region to the overall function of the enzyme is unknown [41, 43]
	Two transmembrane domains near the N-terminus (TMH1-2) and six transmembrane domains (TMH3-8) at the C-terminus	Transmembrane helixes [44]

Protein	Identified conserved domains/motifs/specific amino acids	Predicted functions
	Large cytosolic/catalytic central domain (CD = globular domain = soluble domain), which includes the Plant Conserved Region (P-CR) within Conserved Region 1 (CR1), Class Specific Region (CSR) within Variable Region 2 (VR2) and Conserved region 2 (CR2)	[41, 42, 43]
	Located in the CD domain A consists of several widely spaced aspartic acid (D) residues - a single D followed by a DxD	These residues bind the UDP-glucose substrate. Processive enzymes catalyze the addition of many sugar residues to a growing chain [41, 43]
	Located in the CD domain B consists of a third conserved aspartic acid (D) residue and three conserved amino acids QxxRW.	Part of the catalytic site [41, 43]
LlCOBL4/ LlIRX6	The putative conserved domain characteristic to COBRA superfamily	CDD (NCBI)
	N-terminal signal peptide with cleavage site	Signal peptide cleavage site [45, 46]
	The putative cellulose-binding site	A carbohydrate-binding module (CBM) [46]
	The central Cys-rich (CCVS) motif	Highly conserved and characteristic for all COBL proteins [45, 46]
	Two conserved consensus N-glycosylation sites	Asparagine (N)-linked glycosylation of protein [46]
	Locus corresponds to the predicted cleavage ω-site at the C terminus	Glycosylphosphatidylinositol (GPI) modification motif. GPI anchors are added through an amide bond onto the last amino acid residue remaining after cleavage of the ω-site [46]
LlGAUT12/LlIRX8	N-terminal cytoplasmic domain	Phyre^2
	The transmembrane domain	Phyre^2
	The specific glycosyl transferase family 8 (GT8) domain	Transfer sugar residues to donor molecules. CDD (NCBI)
	The catalytic DxD motif	CDD (NCBI)

Protein	Identified conserved domains/motifs/specific amino acids	Predicted functions
LlPG/ LlQRT	Four typical conserved domains I, II, III and IV	The well-conserved positively charged domain IV (RIKT) constitutes a likely candidate for ionic interactions with carboxylate groups present in the substrate [47, 48, 49]
	Three aspartic acids (D) in domains I and II	The carboxylate group in aspartic acids in NT**D** and **DD** structures (domains I and II, respectively) may be a component of the catalytic site [50]
	The histidine residue (H) in domain III	Participates in catalytic reaction [51]
	A tyrosine (Y) at position 320	Catalytically important in PGs [52]
	12 cysteine (C) residues	Important to maintain the three-dimensional structure of extracellular proteins and are distributed all along the sequences but with a higher frequency at the C-terminal end [49]
LlPCS1	Two motif in both N (DTGS) and C (DS/LGT)-terminal ends characteristic for pepsin like aspartic proteases	Catalytic motifs (CDD, NCBI)
	Two catalytic residues (D)	Plays key catalytic roles in the pepsin family and conserved for all family members (CDD, NCBI)
	Active site flap ATLS and SSSS	An extended loop projecting over the cleft to form an 11-residue flap, which encloses substrates or inhibitors within the active site. It also contribute three residues for substrate specificity (CDD, NCBI)
	Pepsin A like plant domain	Characteristic for chloroplast nucleoids DNA-binding protease and nucellin, pepsin-like aspartic proteases (CDD, NCBI)

Protein	Identified conserved domains/motifs/specific amino acids	Predicted functions
	TAXi_N domain; TAXI_C domain Xylanase inhibitor	The N- and C-termini of the members of this family are jointly necessary for creating the catalytic pocket necessary for cleaving xylanase (cell-survival processes) (CDD, NCBI)
LlGA3ox	Gibberellin 3-β-dioxygenase domain	CDD (NCBI), [53]
	2-oxoglutarate (2OG) and Fe(II)-dependent oxygenase (Oxy) superfamily domain	CDD (NCBI)
	The His-x-Asp-(x)n-His (HxD…H) and Arg-x-Ser (RxS) motifs	Recruit Fe(II) as a cofactor and co-substrate CDD (NCBI)
LlGA2ox1	Gibberellin 2-β-dioxygenase domain	CDD (NCBI)
	Domain characteristic for 2-oxoglutarate (2OG)-Fe(II)-dependent oxygenase superfamily	CDD (NCBI)
	The HxD…H and RxS motifs	Amino acid residues presumed to bind Fe^{2+} at the active site of protein
LlGAMYB	R2R3 domain	Near the 5' terminus
	Box1, Box2, Box3 domains	Distributed throughout the protein
	REB1 domain	Characteristic for Myb superfamily proteins, including transcription factors and mRNA splicing factors
	Myb_DNA-binding domain and SANT (SWI3, ADA2, N-CoR and TFIIIB') domains	DNA-binding domains have been designated using CDD (NCBI)

The complete cDNA sequence of *Ll-MIR159* was identified in yellow lupine (Fig. S10). Then *Ll-MIR159* was compared to *MIR159* sequences cloned in other plant species and showing the highest similarity. On this basis the phylogenetic tree was constructed (Fig. 8D). Further *Ll-MIR159* analyses revealed very high similarity of the 21-nt fragment which form a mature miRNA to another identified in different plant species. In 11 of the 12 species compared, these fragments of sequences were 100% identical (Fig. 8E). Secondary stem-loop structure of the Ll-pre-miR159 and localization of mature miR159 on the stem of the precursor sequence were presented (Fig. 8F). Alignment of the nucleotide sequences of Ll-pre-miR159 with a mature miR159 in *Manihot esculenta*, *Dimocarpus longan*, *Populus trichocarpa*, *Populus tomentosa*, *Cucumis melo*, *Citrus sinensis* and *A. thaliana* was shown (Fig. 8G). Alignment of part of

nucleotide sequences of *LIGAMYB* (Ll-miR159 target gene) with homologous genes from *Glycine soja*, *G. max* and *A. thaliana* was also presented (Fig. 8H).

Discussion

Changes in the yellow lupine anther structure during dehiscence program

Dehiscence of anther is a multistage process which was examined in such species as *A. thaliana*, *O. sativa*, *Zea mays*, *Nicotiana tabacum* and *Solanum lycopersicum* [4]. In our previous study we showed that yellow lupine anther opening takes place in the fourth stage of flower development [34]. Therefore, it seems interesting to study the process of late anther development and the accompanying alterations in tested species. In this paper we have established that the anther wall consists of epidermis, endothecium, middle layers and tapetum, similarly to other plant species. The yellow lupine epidermis protects all anther tissues and develops the stomium, which acts as the site for anther opening, whereas the modifications of endothecium play a critical role in pollen release. The other anther tissues in yellow lupine act in similar manner as in several plant species, hence it follows that the anther dehiscence process is widely preserved (compared to *A. thaliana*, tobacco, tomato, rice and maize) [1, 4, 8, 10, 54, 55]. Nevertheless, there are certain exceptions [12]. Unlike yellow lupine, where the processes of stomium breakage and anther opening are connected in time, in some species like *Allium triquetrum*, these processes are separated. After the rupture of both stomium simultaneously, each *A. triquetrum* whorls still do not fully open and pollen is not released due to the unbroken epidermal cells [56].

Yellow lupine anther endothecium undergoes deposition of lignocellulosic secondary thickening

Secondary thickening of endothecial cell walls occur in four basic types depending on the species: (I) annular ribs, (II) helical ribs forming a pattern of U-shaped thickening, (III) reticulate ribs and (IV) palmate ribs [4, 11]. Some species may have two types of thickenings, but usually the walls of the endothecium show only one type [11]. For example, in *A. triquetrum* there is helical and U-shaped, while in Crocus (Iridaceae) species the thickenings are modified in the form of repeated continuous rings [56, 57]. The location and shape of endothecium can also vary in species-specific manner. In yellow lupine, the endothecium partially surrounds the locule, in tomato the endothecium is located in the upper third of the anther [54], while in the case of maize the endothecium adhered circularly to locule [4, 58]. Additionally, in yellow lupine, secondary thickenings are mainly found in endothecial cells (much less in connective), while in certain species secondary thickenings are also found in other types of anther cells. *A. triquetrum* has thickenings in the endothecium, as well as in the cells of the septum and the connective tissue surrounding the locules [56]. In some species, the epidermis with thickening may perform a function similar to that of the endothecium, thereby providing mechanical force to support the anther opening [59]. It is also known that the dehiscence mechanisms can also be variable, both among families and within a given family. The opening of the anther may be caused via cell lysis and/or mechanical force, and with the aid of secondary cell wall thickening and desiccation, the stomium ruptures releasing pollen grains.

The present of the lignin in the endothecium layer determine the formation of secondary cell wall thickening. In most species, the specific enzyme involved in the biosynthesis of lignin monomers is CAD, which converts cinnamyl aldehydes into their corresponding alcohols. The *A. thaliana* mutant lacking

CAD displays male sterility, and comparing it with the wild type (WT) plants the lignin content is reduced, and the lignin structure is greatly disrupted [14]. All these changes cause that this sterile mutant, due to the lack of lignification of the endothecium, does not produce secondary thickenings, and hence does not release pollen. In our paper we examined the transcriptional activity of *LlCAD* during late development of yellow lupine anthers. The highest level of *LlCAD* expression was found in the first and second selected phases in which the process of endothecial cell wall lignification takes place. About 20 times more gene transcripts were found compared to the third and fourth LAD stages. This suggests that *LlCAD* participates in the lignin biosynthesis in the tissues of yellow lupine anthers.

In addition to the lignification of the endothecium, the cellulosic thickenings are also essential for anther dehiscence. The mutation of *A. thaliana CesA8/ IRX1* gene responsible for the synthesis of cellulose, do not affect formation of primary cell wall thickening, which allows to consider this gene as a specific marker for secondary thickening [15, 16]. In yellow lupine, the expression of *LlIRX1/ LlCesA8* was very high in first two stages of LAD. This closely correlates with the transcriptional activity of *LlCAD* and other identified genes - *LlIRX6/ LlCOBL4* and *LlIRX8/ LlGAUT12*. In general, *COBL* genes, which encode a plant-specific glycosylphosphatidylinositol (GPI) anchored proteins, are key regulators in the deposition of cellulose in secondary cell wall [60]. In turn, xylan- and pectin-deficient *irx8* has mutated *GAUT12* gene, the loss of which results in reduction of G lignin, changes in its deposition, and finally no splitting anthers [18]. Summing up, the identified genes in yellow lupine anthers show co-expression pattern which ensures the proper production of secondary thickening. The obtained results also prove the lignocellulosic nature of the secondary cell walls thickening of endothecium cells in tested species.

Different phytohormones control the formation and deposition of secondary thickening in many plant species. For example, cytokinins (CKs) have been implicated in the regulation of secondary wall formation, since AHP4 (Arabidopsis Histidine-containing Phosphotransfer4), which is element of CK signaling, negatively regulates thickening in the endothecium [61]. Additionally, the transcriptional activity of *AHP4* corresponds to *IRX1/ IRX6/ IRX8* expression, which indicates that CKs control the cellulose biosynthesis [4, 61]. To date, little is known about the effect of GAs on the formation of secondary thickening; therefore, it became the subject of our research. The impact of this phytohormone treatment on the expression of all secondary thickening-related genes was very similar and consisted in increasing the number of transcripts, especially in the second and third LAD phases. In *Cucumis melo* several hormone-responsive cis-regulatory elements in the *CAD* promoter region, including GARE, TATC-box and P-box characteristic for GAs, were identified [40]. It also confirms the important role played by the GAs in the comprehensive program leading to anther opening.

The septum/stomium is enzymatically lysed and undergoes a PCD-mediated degeneration

In yellow lupine anthers, separation of the septum from the stomium cells seems to occur by mechanism similar to organ abscission process, which involves enzymatic lysis of the middle lamellae between the cells without their damaged [35]. In our study, the expression profile of the *LlQRT2* gene encoding marker enzyme involved in rupture the pectin between cells during LAD in yellow lupine was presented. It turned out that the transcript amount was the highest when septum and stomium breakdown occurred (first and second LAD phases, respectively). If dissociation would be mechanical, e.g. by stretching of expanding

anther walls, it damaged the cells involved [57]. Ogawa et al. (2009) have shown that the regulation of cell separation events involves combinations of PGs and phytohormones [19]. *A. thaliana* and tomato *pg* mutants show delay or block anther dehiscence, hence it is known that the role of cell wall enzymatic lysis is important [19, 62]. Additionally, transcriptional activity of *A. thaliana PG - QRT2* is regulated by JA, ET and ABA [19]. In turn, in yellow lupine it has been revealed that GA_3 along with ET precursor regulate functioning of the flower abscission zone; however GA_3 acts independently of ABA in this process [33]. In this paper we demonstrated that the amount of *LlQRT2* transcripts was positively controlled by GA_3. The level of *LlQRT2* mRNA increased, especially in the second LAD phase, which suggests the GA-dependent modulation of the septum/stomium interruption in the studied plant. Data on the impact of GAs on *PG* expression in different plant species are lacking. In *A. thaliana* anthers, the application of other phytohormone - JA causes the increase of *QRT2*, *ADPG1* (*ARABIDOPSIS DEHISCENCE ZONE POLYGALACTURONASE1*) and *ADPG2* expression about 10 times [19]. In wheat (*Triticum aestivum*) cis-acting elements in promotor sequences of *TaPGs* genes were predicted. What is important, they included cis-elements regulated by phytohormones and transcription factors, such as abscisic acid (ABRE), gibberellin (P-Box), auxin (TGA-element), methyl jasmonate (CGTCA, TGACG), and MYB binding site involved in drought-inducibility (MBS). Similar research was carried out in *Brassica oleracea*, and the hormone-response cis-elements were also found for MeJA (CGTCA), auxin (TGA-box and AuxRR-core), GA (GARE, P-box, TATC-box), salicylic acid (TCA-element), and abscisic acid (ABRE) [63].

The separated septum cells of yellow lupine further progressively degenerate. Septum degenerates first to create a bilocular anther, and the stomial cells then degenerate to break the anther wall. In other plant species these processes occurring in specified cells are aided by PCD [1, 8]. Ge et al. (2005) showed that PCD inhibitory factor *PCS1* encoding aspartic protease acts in the endoplasmic reticulum and functions to promote cell survival during embryogenesis and gametogenesis. *PCS1* is not constantly expressed in tissues but is involved in various specific developmental processes. A characteristic pattern of *PCS1* expression has been demonstrated in developing flowers, young siliques, and also in anther. Further analyzes revealed the presence of *PCS1* mRNA in pollen and anther wall, with the exception of tapetum layer, where no information has been provided [21]. Overexpression of *PCS1* in *A. thaliana* anther results in inhibition of dehiscence process, therefore we focused on establishing the expression of this gene in yellow lupine tissues. Our results showed that the level of *LlPCS1* fluctuates at different stages of LAD. It seems extremely interesting to find that *LlPCS1* transcriptional activity is controlled by GA_3. As expected, hormone molecules reduce the amount of *LlPCS1* mRNA, especially in the first and fourth LAD phases, which indirectly proves the GA-dependent manner of septum/stomium cell degeneration in yellow lupine. Summing up, obtained results suggests that PCD-related processes take place during the development of yellow lupine anthers, but the mechanisms of these strictly controlled processes require further research. In various plant species, two main types of stomium rupture were recognized: (1) basic mechanical breakage and (2) active PCD-related degeneration [8, 9, 64]. In longitudinally dehiscing anthers, a mechanical opening of anthers has been proposed, while in other species, including *Crocus boryi*, the basis of anther rupture is the occurrence of certain changes characteristic for PCD (nuclear pycnosis, cell collapse) [57, 64]. The developmental PCD is also controlled by phytohormones. Sanders et al. (2000)

showed that the mutant associated with the JA biosynthetic pathway - *opr3* is characterized by a delay in the degeneration of stomium cells, which finally disturbs anther dehiscence [9]. Indirectly, it is a strong proof of the involvement of these phytohormones in PCD and at the same time in the process of anther opening. However, further investigations are needed to understand the full mechanism of this process.

Gibberellins are essential modulators of the anther dehiscence in yellow lupine

The multi-functionality of GAs in the early stages of anther development, mainly tapetum and pollen, is well documented through analyzes of *A. thaliana* and rice mutants. However, the late stages of anther development related to their final split, has not been well understood due to the earlier GA-deficiency mutant disturbances that prevent further anther development [65]. In yellow lupine, studies on expression profile have shown that fluctuating transcript level of *LlDELLA1*, which encodes the main repressor of GA signaling, promotes proper flower and pod development. *LlDELLA1* mRNA level is lowest when the anthers are opened and then increases during the fertilization and early pod developmental stages [34]. These results encouraged us to investigate the localization of GA_3 in selected stages of late anther development in yellow lupine. Our results obtained in this work closely correlate with the expression pattern of the *LlDELLA1* gene, in the opposite manner. The highest accumulation of GA_3 occurs in the first LAD phase that is before anther opening. The GA_3 signal was observed mainly in degenerating septum cells, near the vascular bundle, in the middle layer, endothecium, as well as in the epidermis but less often. In the second LAD phase, where the stomium cells are disrupted and the pollen chambers are opened, a fluorescence signal was almost unnoticeable; whereas no signal was found in third and fourth LAD stages. In the case of rice, GA_4 accumulation was found to be highest in anthers just before anthesis. The level of active hormone molecules decreased and a week after anthesis was completely undetectable in the young seeds [66]. These results suggest that GAs play an important role in specific organs (place) at a specific stage of the life cycle (time), and that they may be concerned with the strictly regulation of reproductive growth and development in different species.

The application of GA biosynthesis inhibitor - PAC in petunia (*Petunia hybrida*) causes male sterility resulting from inhibition of anther development in post-meiotic phase. Detailed analyzes showed that connective and tapetum were degenerated, but pollen grains were still present. In petunia transgenic plants with overexpression of GA signaling repressor *AtSPY* the anther phenotype was comparable to that observed after PAC treatment [67]. At present, it is known that in some plants, inhibition of GA biosynthesis blocks anther development after meiosis, (petunia, *A. thaliana*, maize), but in others, blockage occurs before meiosis, i.e. tomato [65]. The key and final gene involved in GA biosynthesis is *GA3ox*. We showed that the transcriptional activity of *LlGA3ox* strictly correlates with GA_3 localization in yellow lupine during late anther development. The highest number of *LlGA3ox* transcripts was found in the first and second LAD stages, which decreased significantly in the third and fourth stages. Moreover, after the application of PAC, the amount of *LlGA3ox* mRNA decreases by more than half, mainly in the first three selected phases. This suggests that this particular *LlGA3ox* gene may be involved in the synthesis of bioactive phytohormone molecules that play an essential role in the studied process in yellow lupine. In addition, we demonstrated that the expression of *LlGA2ox1* encoding the enzyme responsible for GA inactivation shows an opposite expression to *LlGA3ox*. The role of genes involves in

the GA biosynthesis and inactivation during stamen development is well understood in many plant species. The transcriptional activity of *AtGA3ox1-AtGA3ox4* genes was found specifically in stamens, and additionally *AtGA3ox1* is also expressed in some other floral organs. Both the stamen filaments and anthers require GAs for proper development, and *de novo* synthesis of this hormone was confirmed at both sites. The transcript of *AtGA3ox1* was found in the filament, while *AtGA3ox2-AtGA3ox4* are expressed in anthers and pollen [26]. GAs, mainly GA_4, need to be transported from stamens or flower receptacle to other floral organs to ensure proper development. Despite the lack of expression of all the *AtGA3ox* genes in the petals, it turned out that the mutant deficient in the *AtGA3ox1* and *AtGA3ox3* showed serious defects in the petal development [26]. In yellow lupine anther, this idea could be explained by the observation of a fluorescent signal indicating the presence of GA_3 in the cells of the conductive bundle. Therefore, there is a high probability that the active phytohormone molecules are transported from the anther to the filament or vice versa. An analogous situation was observed in petunia where GA application restored normal corolla pattern, previously disturbed by removal of the stamens [68]. Similarly anther expression patterns of *GA3ox* genes were also observed in tobacco and rice [69, 70]. Summing up, stamens are a key source of GAs in flowers in different plant species. Besides their local influence on the stamen development, their transport to adjacent tissues of the flower organs is equally important [26].

GAMYB transcription factor mediates GA signal transduction in aleurone tissues of cereals. Furthermore, it is necessary in ensuring the fertility of anthers in many species. Similarly to GA biosynthesis mutants, *gamyb* demonstrates the impact of the GA signaling on the early stages of anther development. Mutation in the *GAMYB* in rice and double mutation of *MYB33* and *MYB65* in *A. thalian*a interrupt PCD causing abnormal enlargement of tapetum cells, which finally disorders the pollen development [28]. However, there is a little data concerning the role of *GAMYB* in late anther development. In this paper, we examined yellow lupine *LlGAMYB* expression in selected phases of LAD, and after GA_3 and PAC application. The *LlGAMYB* transcript level was almost identical with or without GA_3 treatment, but PAC application resulted in increased *LlGAMYb* mRNA, especially in first and second LAD phases. This suggests that GA_3-dependent pathway perhaps controls *LlGAMYB* expression but not in direct manner. It can be assumed only that the presence of GA_3 blocks the transcription factor, which positively regulates the expression of *LlGAMYB*, but the exact mechanism requires further research. The results obtained in other plant species show that *HvGAMYB* in barley and *GAMYB-like* genes in *A. thaliana* are expressed in flowers and are positively regulated by GAs [29, 71]. It follows that the role of *GAMYB* in GA-regulated gene expression during anther development differs between species. Moreover, the function of *GAMYB* also varies within a species between developmental processes, e.g. seed germination, vegetative and reproductive development [72]. Very interesting are the results of studies carried out on barley, which indicate that transgenic plants strongly overexpressing *HvGAMYB* in anthers are completely male sterile. This phenotype was characterized by an intact septum [29]. Taking into account our results obtained in yellow lupine, where we observed the highest level of GA_3 in the progressively degenerating septum cells, it can be concluded that the presence of GA_3 at this stage of anther development strictly regulates the level of target gene transcripts (establishing a certain balance), which results in a specific and correct physiological response. Pollen of *HvGAMYB*-overexpressing barley anthers has a specific phenotype [29].

The development of slightly smaller and irregular pollen is normal, and moreover, some pollen has been shown to be viable. The observed male sterility is mainly due to disrupted anther wall tissues, which do not break [29]. Similar to barley, a phenotype of small, indehiscent anthers was observed in wheat after GA_3 treatment [73, 74]. The occurrence of male sterility following application of GA_3 in wheat, in conjunction with the observation that (1) *HvGAMYB* overexpression causes indehiscence anther and that (2) *LlGAMYB* expression is relatively constant after GA_3 application but increases after PAC treatment, let suppose that *GAMYB* play specific role during anther development in species-specific manner. This requires further research and more clarification.

Many reports have suggested that expression of the *GAMYB-like* genes in *A. thaliana* is regulated post-transcriptionally by a microRNA (miRNA) named miR159 [30, 75]. miR159 is small (21 nt), non-coding RNA sequence derived from double-stranded RNA (dsRNA). At-miR159 affects the transcriptional activity of its target genes, including *AtMYB33*, *AtMYB65* and *AtMYB101* [30]. In rice, Tsuji et al (2006) reveled that miR159 regulates the transcript level of *GAMYB* only in flowers, and this situation was not observed in aleurone cells. It follows that the regulation of *GAMYB* expression and its function is organ specific [72]. Due to this fact and also to find a factor that may determine the level of *LlGAMYB* transcripts during anther development of yellow lupine we examined *LlMIR159* expression after GA_3 and PAC application. Interestingly, the GA_3 treatment increased the *LlMIR159* transcript content, and PAC application significantly decreased its amount. The observed expression profile of *LlMIR159* partially explains the transcriptional activity changes observed for *LlGAMYB* after different compounds application. The obtained results also indicate that the expression of the *LlMIR159* gene is regulated via GA signaling pathway. A similar situation occurs in *A. thaliana*, where GAs regulate miR159 level [30]. In the flowers of GA biosynthesis mutant *ga1-3*, there was significantly less miR159 compared to the WT flowers. Application of GAs to the flowers of the mutant increased the level of miR159 to a level comparable to that of GA-treated WT plants, and what's more, this level was higher than that of untreated WT plants. Due to the reduced level of *AtMYB33*, plants overexpressing miR159 showed male sterility and delayed flowering [30]. As demonstrated by the experiments with the *GUS* reporter gene, the localization of AtMYB33:GUS encoded by gene with the complete miR159 target sequence was only in young anthers, whereas the AtMYB33:GUS was expressed in various flower organs when gene possessed damage in the miR159 target sequence [75].

By analyzing the natural conditions without the application of any compounds, it can be concluded that *LlGAMYB* expression remains at a higher level in the first two stages of LAD and then decreases. This negatively correlates with the transcriptional activity of the *LlMIR159*, which was significantly increased in the second phase of LAD. This is probably the cause of the reduced mRNA content of the *LlGAMYB* in third and fourth LAD stages. The obtained results suggest that *LlGAMYB* is co-expressed with *LlMIR159* in yellow lupine anthers. It also follows that *LlGAMYB* gene is regulated by miR159 in anther of yellow lupine.

In silico analyses

In this paper, nine full-length cDNA sequences of genes related to the anther dehiscence process in yellow lupine have been identified. The implemented methodology was successful for identification and characterization of conserved domains, motifs and specific amino acids of all predicted proteins. This approach made it possible to predict and assign them specific functions. The identified genes encode functional proteins closely related to Fabaceae family. Moreover, protein multiple alignments provided information about conservation of sequences in many plant species. It also allows for the specification of fragments of protein sequences which are the most crucial for the function they perform. In turn, the construction of phylogenetic trees allowed for conclusions about the origin of the predicted yellow lupine proteins.

Based on bioinformatics and experimental results of research, miR159 mediates regulation of family of *GAMYB* and *GAMYB-like* genes in varied plant species, including *A. thaliana* [75], rice [72] and strawberry [76]. All of these *GAMYB* genes from different plant species, and also *LlGAMYB* identified in this work from yellow lupine, contain a conserved miR159 binding site, which is highly complementary to their corresponding miR159 sequence and located in the conserved region between BOX1 and BOX2 of the *GAMYB* genes [72, 75]. This indicates that the miR159-*GAMYB* pathway is conserved across species.

Conclusions

This paper advances knowledge about the hormonal and molecular regulation of late anther development in yellow lupine (*Lupinus luteus* L), which will be an important aspect of controlling fertility in this valuably legume crop species. We showed that the anther split is complex process involving formation and deposition of lignocellulosic secondary thickening in the endothecium, enzymatic breakdown of cell walls at the septum/stomium, cell degeneration via PCD-related processes and finally stomium rupture resulting in pollen release. Time-varying expression of the identified genes being markers of developmental changes during anther dehiscence is also regulated in a GA dependent pathway. Tissue and cellular localization showed that GA_3 is essential modulator of the dehiscence process, especially in the time prior to anther opening. The appropriate GA_3 level, which correlates with GA metabolism, at the right time and place controls the yellow lupine anther opening likely through the influence on *LlGAMYB* expression via *Ll-MIR159*-dependent pathway. Therefore, the yellow lupine anther dehiscence is highly regulated, enabling the timing of pollen release to be tightly controlled to maximize the chances of fertilization.

Methods

Plant material, growing conditions and compounds treatments

The plant material was yellow lupine (*Lupinus luteus* L.) cv. Taper. Obtained from the Plant Breeding Station Wiatrowo (Poland) the seeds were prepared and sown as described by [34] in the experimental field in Pędzewo, Kuyavian-Pomeranian Voivodeship in north-central Poland (53°05'02"N 18°21'28"E). The plants were cultivated on the 5th soil class as recommended by the manufacturer. The anthers from

particular stages of late development (1–4 LAD, Fig. 1A) were dissected from flowers with a sharp scalpel. For each phase of LAD not less than 80 plants were used, and additionally, part of the collected material was previously treatment with gibberellic acid (GA_3, 100 μM) or GA biosynthesis inhibitor – paclobutrazol (PAC, 100 μM) in a 0.05% Tween 20 solution using a sprayer. The anthers in the corresponding developmental phases were used as control group, and they were treated with 0.05% Tween 20 solution only. According to the planned experiment, 3 h after applications the anthers were harvested and processed fresh or frozen in liquid nitrogen (then stored at -80 °C until use).

Identification of cDNAs

The cDNA sequences of individual genes have been identified differently. Molecular cloning of *LlGA2ox1* cDNA was performed as described by [33]. The identification of *LlGAMYB* cDNA was as follows: the 1 g of yellowish-green flowers was pounded in liquid nitrogen using a mortar and pestle. Then, according to the manufacturer's instructions, total RNA was isolated by the column method (NucleoSpin® RNA kit, Macherey-Nagel, Düren, Germany), while the reverse transcription was made using 1 μg of RNA, oligo$(dT)_{18}$ primers, and Transcriptor High Fidelity cDNA Synthesis Kit (Roche, Mannheim, Germany). Touchdown PCR was performed using 1.25 U Perpetual Taq DNA Polymerase$^{HOT\ START}$ (EURx, Gdańsk, Poland), 2 μl of first-strand cDNA, 1 x buffer B, 0.2 mM dNTP mix, 3.0 mM Mg^{2+}, 1 μM degenerated primers (Tab. S1) and deionized water (up to final volume of 50 μl) in the T3 Thermocycler (Biometra, Göttingen, Germany). An amplified cDNA fragment (704 bp, Fig. S11A) was isolated and purified from an agarose gel (GeneMATRIX Agarose Out DNA Purification Kit, EURx). In the insertion site, PCR product was ligated into the pCRII-TOPO vector (Fig. S11B, TOPO TA Cloning Kit, Invitrogen, Carlsbad, USA), and transferred into One Shot Mach1-T1 *E. coli* in the form of plasmid. The bacterial cells were plated on Petri dishes, which contained S-Gal/LB Agar Blend (Sigma-Aldrich, St. Louis, MO, USA) with addition of ampicillin (50 μg/ml) (Fig. S11C). Unlike the dark blue bacterial colonies, white ones were selected and cultured in liquid LB medium with ampicillin (50 μg/ml) for 12 h. Finally, in accordance with the manufacturer's guidelines, the plasmid DNA was isolated (GeneMATRIX Plasmid Miniprep DNA purification kit, EURx), digested with the restriction enzyme *Eco*RI (Fermentas) (Fig. S11D), and sequenced by Genomed (Warsaw, Poland). The 485 bp (Fig. S12A) and 768 bp (Fig. S12B) fragments were obtained from the 3'RACE-PCR (FirstChoice RLM-RACE Kit, SuperTaq-Plus Polymerase, Ambion, Austin, USA) with using two different pairs of primers (Tab. S1). The amplicons were isolated, purified, cloned, digested (Fig. S12C/D) and sequenced as described above. Due to difficulties arising from the experimental identification of the 5' end of *LlGAMYB* cDNA, it was obtained based on sequences derived from a later RNA-Seq experiment deposited at NCBI in the Sequence Read Archive (SRA) database under accession number PRJNA285604 (BioProject) [77] and experiment accession number SRX1069734. All fragments had overlapping nucleotide sequences which allowed obtaining the complete *LlGAMYB* sequence. *De novo* assembled transcriptome of yellow lupine from RNA-seq experiment was also used to identify *LlCAD*, all *LlIRXs*, *LlQRT2*, *LlPCS1*, *LlGA3ox1* and precursor of Ll-miR159 (*Ll-MIR159*).

Expression analysis

Quantitative real-time PCR (qPCR) was used to establish the expression pattern of all identified genes. 80 mg of frozen anthers (being at a specific stage of development with or without GA_3/PAC treatment) were homogenized in a sterile mortar with a pestle. According to the manufacturer's instructions, first total RNA using Isolate II RNA Plant Kit (Bioline, London, UK) was isolated, and next reverse transcription with matrix (2 µg), oligo$(dT)_{18}$ (Roche) and the Transcriptor High Fidelity cDNA Synthesis Kit was performed. qPCRs were carried out using LightCycler 2.0 Carousel-Based System (Roche) in 20 µl capillaries which contained the mix of 0.1 µg of cDNA, 0.2 µM gene-specific primers (Tab. S1), 0.05 µM Universal Probe Library (UPL) hydrolysis probes (Roche) (Tab. S1), 1 × LightCycler TaqMan Master Mix (LightCycler TaqMan Master Kit, Roche) and H_2O. The following program was used: 600 s at 96 °C; 45 cycles of 10 s at 96 °C, 20 s at specific annealing temperature (Tab. S1), 1 s at 72 °C; and 30 s at 40 °C. The negative no template controls (NTC) were included. As an endogenous control the actin gene (*LIACT*, GenBank accession number KP257588) was selected [32, 33, 34]. The absolute quantification was designed from the serial dilutions of cDNAs generating standard curves, whereas the relative gene expression (the data of the studied gene relative to internal control gene and calibrator) was determined using the 2 (-DeltaDeltaC(T)) method [78].

Histological studies

A fixer containing 4% paraformaldehyde (w/v), 0.2% glutaraldehyde (v/v) and 3% N-ethyl-N'-(3-dimethylaminopropyl)carbodiimide hydrochloride (EDAC) (w/v) (Sigma-Aldrich) in 1 × phosphate-buffered saline buffer (1 × PBS, pH 7.2) was prepared and applied into appropriate anther tissue small fragments for 12 h at 4 °C. Samples were washed out of fixative in triplicate with 1 × PBS (pH 7.2) for 10 min. Dehydrated was achieved by placing the material in increasing ethanol concentrations (30%, 50%, 70%, 90%, 100%) (v/v). Then, supersaturation and embedding in BMM resin (butyl methacrylate, methyl methacrylate, 0.5% (w/v) benzoin ethyl ether, 10 mM dithiothreitol) (Fluka, Buchs, Switzerland) were performed at − 20 °C under UV light. Using the ultramicrotome (Reichert-Jung, Germany) semi thin sections have been received, which were later placed on slides, stained with 0.05% toluidine blue (Sigma-Aldrich), and observed under LM Zeiss Axioplan (Carl Zeiss, Oberkochen, Germany) microscope with a ProGres C3 digital camera.

GA_3 immunolocalization

The anther tissue fragments were fixed, washed, dehydrated, supersaturated, embedded, polymerized and cut in the same way as described for histological studies. Next, semi thin sections were placed on slides with Biobond (BBInternational, Cardiff, UK), and after washing off the resin blocked in BlockAid TM Blocking Solution (Thermo Fisher Scientific, Waltham, MA, USA) according to the manufacturer's instruction. Then, sections were incubated with polyclonal primary antibody anti-GA_3 (Abbexa, Cambridge, UK) diluted 1:50 in 1% bovine serum albumin (BSA) in 1 × PBS (pH 7.2), and placed in a wet container at 4 °C for 12 h. Next, the primary antibodies by washing 3 times in 1 x PBS (pH 7.2) were removed and secondary antibody (MFP488 goat anti-rabbit IgG, MoBiTec, Goettingen, Germany) diluted 1:250 in PBS buffer were applied for 2 h at 37 °C. A negative control was done by omitting the incubation

with primary antibody (Fig. S13). The next step was the incubation with DAPI (1:2500) for 10 min., and washing it out with distilled water. Finally, the samples were observed in a Leica DMI4000B inverted microscope using the BP365, FT395, and LP397 filters.

Is silico analyses

The integrated FastPCR v.6.5.99 [79] tool was used for degenerate and RACE-PCR primers design. The Universal Probe Library Assay Design Center [80] was used for design of qPCR specific primers and short hydrolysis UPL probes substituted with Locked Nucleic Acids. The identified cDNA sequences of all genes and predicted proteins were analyzed using Basic Local Alignment Search Tool (BLAST) [81] and the bioinformatics resource portal of the Swiss Institute of Bioinformatics [Expasy [82], including Translate tool [83] which allows the translation of a nucleotide sequences to a protein sequences, and ProtParam tool [84] for calculation of molecular weights and isoelectric points]. Alignments and phylogenetic reconstructions were performed using Python Environment for Tree Exploration3 (ETE3) v3.1.1 program as implemented on the GenomeNet [85]. Maximum likelihood phylogenetic trees were inferred using PhyML v20160115 ran with model and parameters: –pinv e -o tlr -f m –bootstrap – 2 –nclasses 4 –alpha e. Branch supports are the Chi^2-based parametric values return by the approximate likelihood ratio test. Multiple alignments of different amino acid sequences found in BlastP and showing close association with yellow lupine sequences were carried out using ClustalW [86] program with default settings. The presence of functional domains were checked via NCBI's Conserved Domain Database (CDD) [87], which is a protein annotation resource, consisting of a collection of well-annotated multiple sequence alignment models for ancient domains and full-length proteins. These are available as position-specific score matrices (PSSM) for the rapid identification of conserved domains in protein sequences via RPS-BLAST. CDD content includes NCBI-curated domains, as well as domain models imported from a number of external source databases (Pfam, SMART, COG, PRK, TIGRFAMs). The cytoplasmic and transmembrane domains were also predicted using TMHMM v. 2.0 [88] and Protein Homology/analogY Recognition Engine V 2.0 ($Phyre^2$) [89] web portal for protein modeling, prediction and analysis. Comparisons of proteins derived from different plant species were made using the DiAlign program (Genomatix) [90] with default parameters. The tertiary structures of the proteins derived from yellow lupine were constructed using protein structure prediction Robetta service [91], which uses the PDB100 template database and a co-evolution based model database (MDB). The obtained results were visualized using the UCSF ChimeraX [92], which is the next-generation molecular visualization program from the Resource for Biocomputing, Visualization, and Informatics (RBVI).

Statistical analysis

All presented data are the results of three separate samples (biological replications) with two repetitions of each (technical replications) and presented as mean ± standard error (SE). Statistical analysis were performed using one-way Anova followed by post-hoc Tukey’s HSD test, with differences accepted at $p < 0.05$. All analyses were performed using R version 3.5.3.

Abbreviations

ACT
actin; ADPG1/2–Arabidopsis dehiscence zone polygalacturonase 1/2; AHP4–Arabidopsis histidine-containing phosphotransfer 4; C–connective; CAD–cinnamyl alcohol dehydrogenase; CesA8–cellulose synthase A catalytic subunit 8 [UDP-forming]; CKs–cytokinins; COBL4–COBRA-like 4; E–epidermis; En–endothecium; GA_3–gibberellic acid; GA3ox–gibberellin 3-oxidase; GA2ox–gibberellin 2-oxidases; GAs–gibberellins; GAUT12–galacturonosyltransferase 12; GPI - glycosylphosphatidylinositol; GT8 - glycosyl transferase family 8; IRX1/6/8–irregular xylem 1/6/8; LAD–late anther development; PAC–paclobutrazol; PCD–programmed cell death; PCS1–promotion of cell survival 1; PG–pollen grain; PGs–polygalacturonases; QRT2–quartet 2; Se–septum; St–stomium; StR–stomium region; T–tapetum; VB–vascular bundle.

Declarations

Ethics approval and consent to participate: Not applicable

Consent for publication: Not applicable

Availability of data and materials: All data generated or analysed during this study are included in this published article and its supplementary information files.

Competing interests: The authors declare that they have no competing interests

Funding: This research was supported by the Polish Ministry of Agriculture and Rural Development [Grant Numbers 149/2011 and 222/2015].

Authors' contributions: Conception and design - KM; Investigations - KM, KP; Analyzes - KM; Writing the manuscript - KM; Preparing the figures and tables - KM, KP; Supervision - KM; Approval for publication - KM, KP.

Acknowledgements: The authors would like to thank Michał Świdziński (Nicolaus Copernicus University, Faculty of Biological and Veterinary Sciences, Department of Cellular and Molecular Biology) for helping with the preparation of ultratinsections for microscopy experiments.

References

1. Sanders PM, Bui AQ, Weterings K, McIntire KN, Hsu YC, Lee PY, et al. Anther developmental defects in Arabidopsis thaliana male-sterile mutants. Sex Plant Reprod. 1999;11:297–322.
2. Scott RJ, Spielman M, Dickinson HG. Stamen structure and function. Plant Cell. 2004;16:46–60.
3. Wilson ZA, Zhang DB. From Arabidopsis to rice: pathways in pollen development. J Exp Bot. 2009;60:1479–92.

4. Wilson ZA, Song J, Taylor B, Yang C. The final split: the regulation of anther dehiscence. J Exp Bot. 2011;62:1633–49.
5. Marciniak K, Przedniczek K. Comprehensive insight into gibberellin- and jasmonate-mediated stamen development. Genes 2019;10:811.
6. Goldberg RB, Beals TP, Sanders PM. Anther development: basic principles and practical applications. Plant Cell. 1993;5:1217–29.
7. Mandaokar A, Thines B, Shin B, Lange BM, Choi G, Koo YJ, et al. Transcriptional regulators of stamen development in *Arabidopsis*identified by transcriptional profiling. Plant J. 2006;46:984–1008.
8. Sanders PM, Bui AQ, Le BH, Goldberg RB. Differentiation and degeneration of cells that play a major role in tobacco anther dehiscence. Sex Plant Reprod. 2005;17:219–41.
9. Sanders PM, Lee PY, Biesgen C, Boone JD, Beals TP, Weiler EW, et al. The Arabidopsis *DELAYED DEHISCENCE1* gene encodes an enzyme in the jasmonic acid synthesis pathway. Plant Cell. 2000;12:1041–61.
10. Matsui T, Omasa K, Horie T. Mechanism of anther dehiscence in rice (*Oryza sativa*). Ann Bot. 1999;84:501–6.
11. Garcia CC. An approach to the diversity of endothecial thickenings in Solanaceae. Flora. 2002A;197:214–23.
12. Garcia CC. Anther wall formation in Solanaceae species. Ann Bot. 2002B;90:701-706.
13. Boerjan W, Ralph J, Baucher M. Lignin biosynthesis. Annu Rev Plant Biol. 2003;54:519–46.
14. Thevenin J, Pollet B, Letarnec B, Saulnier L, Gissot L, Maia-Grondard A, et al. The simultaneous repression of CCR and CAD, two enzymes of the lignin biosynthetic pathway, results in sterility and dwarfism in *Arabidopsis thaliana*. Mol Plant. 2011;4:70–82.
15. Brown DM, Zeef LA, Ellis J, Goodacre R, Turner SR. Identification of novel genes in Arabidopsis involved in secondary cell wall formation using expression profiling and reverse genetics. Plant Cell. 2005;17:2281–95.
16. Taylor NG, Scheible WR, Cutler S, Somerville CR, Turner SR. The *irregular xylem3* locus of Arabidopsis encodes a cellulose synthase required for secondary cell wall synthesis. Plant Cell. 1999;11:769–80.
17. Taylor NG, Howells RM, Huttly AK, Vickers K, Turner SR. Interactions among three distinct CesA proteins essential for cellulose synthesis. Proc Natl Acad Sci USA. 2003;100:1450–5.
18. Hao Z, Avci U, Tan L, Zhu X, Glushka J, Pattathil S, et al. Loss of Arabidopsis *GAUT12/IRX8* causes anther indehiscence and leads to reduced G lignin associated with altered matrix polysaccharide deposition. Front Plant Sci. 2014;5:357.
19. Ogawa M, Kay P, Wilson S, Swain SM. ARABIDOPSIS DEHISCENCE ZONE POLYGALACTURONASE1 (ADPG1), ADPG2, and QUARTET2 are polygalacturonases required for cell separation during reproductive development in Arabidopsis. Plant Cell. 2009;21:216–33.
20. Kuriyama H, Fukuda H. Developmental programmed cell death in plants. Curr Opin Plant Biol. 2002;5:568–73.

21. Ge X, Dietrich C, Matsuno M, Li G, Berg H, Xia Y. An Arabidopsis aspartic protease functions as an anti-cell-death component in reproduction and embryogenesis. EMBO Reports. 2005;6:282–8.
22. Feys BJ, Benedetti CE, Penfold CN, Turner JG. Arabidopsis mutants selected for resistance to the phytotoxin coronatine are male sterile, insensitive to methyl jasmonate, and resistant to a bacterial pathogen. Plant Cell. 1994;6:751–9.
23. Ishiguro S, Kawai-Oda A, Ueda J, Nishida I, Okada K. The *DEFECTIVE IN ANTHER DEHISCHENCE1* gene encodes a novel phospholipase A1 catalyzing the initial step of jasmonic acid biosynthesis, which synchronizes pollen maturation, anther dehiscence, and flow opening in Arabidopsis. Plant Cell. 2001;13:2191–209.
24. Cheng H, Qin L, Lee S, Fu X, Richards DE, Cao D, et al. Gibberellin regulates Arabidopsis floral development via suppression of DELLA protein function. Development. 2004;131:1055–64.
25. Chhun T, Aya K, Asano K, Yamamoto E, Morinaka Y, Watanabe M, et al. Gibberellin regulates pollen viability and pollen tube growth in rice. Plant Cell. 2007;19:3876–88.
26. Hu J, Mitchum MG, Barnaby N, Ayele BT, Ogawa M, Nam E, et al. Potential sites of bioactive gibberellin production during reproductive growth in Arabidopsis. Plant Cell. 2008;20:320–36.
27. Rieu I, Ruiz-Rivero O, Fernandez-Garcia N, Griffiths J, Powers SJ, Gong F, et al. The gibberellin biosynthetic genes *AtGA20ox1* and *AtGA20ox2* act, partially redundantly, to promote growth and development throughout the Arabidopsis life cycle. Plant J. 2008b;53:488–504.
28. Aya K, Ueguchi-Tanaka M, Kondo M, Hamada K, Yano K, Nishimura M, et al. Gibberellin modulates anther development in rice via the transcriptional regulation of *GAMYB*. Plant Cell. 2009;21:1453–72.
29. Murray F, Kalla R, Jacobsen J, Gubler F. A role for HvGAMYB in anther development. Plant J. 2003;33:481–91.
30. Achard P, Herr A, Baulcombe DC, Harberd NP. Modulation of floral development by a gibberellin-regulated microRNA. Development. 2004;131:3357–65.
31. Zheng L, Nagpal P, Villarino G, Trinidad B, Bird L, Huang Y, et al. miR167 limits anther growth to potentiate anther dehiscence. Development. 2019;146:174375.
32. Glazinska P, Wojciechowski W, Kulasek M, Glinkowski W, Marciniak K, Klajn N, et al. *De novo* transcriptome profiling of flowers, flower pedicels and pods of *Lupinus luteus* (yellow lupine) reveals complex expression changes during organ abscission. Front Plant Sci. 2017;8:641.
33. Marciniak K, Kućko A, Wilmowicz E, Świdziński M, Przedniczek K, Kopcewicz J. Gibberellic acid affects the functioning of the flower abscission zone in *Lupinus luteus* via cooperation with the ethylene precursor independently of abscisic acid. J Plant Physiol. 2018;229:170-4.
34. Marciniak K. Przedniczek K. Gibberellin signaling repressor *LlDELLA1* controls the flower and pod development of yellow lupine (*Lupinus luteus*). Int J Mol Sci. 2020;21:1815.
35. Kućko A., Smoliński D., Wilmowicz E., Florkiewicz A., de Dios Alché J. Spatio-temporal localization of *LlBOP* following early events of floral abscission in yellow lupine. Protoplasma 2019; 256, 1173–83.

36. Bonawitz ND, Chapple C. The genetics of lignin biosynthesis: connecting genotype to phenotype, Annu Rev Genet. 2010;44:337–63.
37. Taylor NG, Laurie S, Turner SR. Multiple cellulose synthase catalytic subunits are required for cellulose synthesis in Arabidopsis. Plant Cell. 2000;12:2529–39.
38. Galeano E, Vasconcelos TS, Carrer H. Characterization of *Cinnamyl Alcohol Dehydrogenase* gene family in lignifying tissues of *Tectona grandis* Silvae Genet. 2018;67:1–11.
39. Tang R, Zhang XQ, Li YH, Xie XM. Cloning and *in silico* analysis of a cinnamyl alcohol dehydrogenase gene in *Pennisetum purpureum*. J Genet. 2014;93:145–58.
40. Jin Y, Zhang C, Liu W, Qi H, Chen H, Cao S. The cinnamyl alcohol dehydrogenase gene family in melon (*Cucumis melo*): bioinformatic analysis and expression patterns. PLoS One. 2014;9:e101730.
41. Richmond T. Higher plant cellulose synthases. Genome Biol. 2000;1:3001.1–3001.6.
42. Hill JL Jr, Josephs C, Barnes WJ, Anderson CT, Tien M. Longevity in vivo of primary cell wall cellulose synthases. Plant Mol Biol. 2018;96:279–89.
43. Olek AT, Rayon C, Makowski L, Kim HR, Ciesielski P, Badger J, et al. The structure of the catalytic domain of a plant cellulose synthase and its assembly into dimers. Plant Cell. 2014;26:2996–3009.
44. Slabaugh E, Davis JK, Haigler CH, Yingling YG, Zimmer J. Cellulose synthases: new insights from crystallography and modeling. Trends Plant Sci. 2014;19:99–106.
45. Sindhu A, Langewisch T, Olek A, Multani DS, McCann MC, Vermerris W. Maize *Brittle stalk2* encodes a COBRA-Like protein expressed in early organ development but required for tissue flexibility at maturity. Plant Physiol. 2007;145:1444–59.
46. Gao Y, Bian L, Shi J, Xu J, Xi M, Wang G. Expression of a conifer COBRA-like gene *ClCOBL1* from Chinese fir (*Cunninghamia lanceolata*) alters the leaf architecture in tobacco. Plant Physiol Biochem. 2013;70:483–91.
47. Bussink HJD, Buxton FP, Visser J. Expression and sequence comparison of the *Aspergillus niger* and *Aspergillus tubigensis* genes encoding polygalacturonase II. Curr Genet. 1991;19:467–74.
48. Tebbutt SJ, Rogers HJ, Lonsdale DM. Characterization of a tobacco gene encoding a pollen-specific polygalacturonase. Plant Mol Biol. 1994;25:283–97.
49. Torki M, Mandaron P, Mache R, Falconet D. Characterization of a ubiquitous expressed gene family encoding polygalacturonase in *Arabidopsis thaliana*. Gene. 2000;242:427–36.
50. Rexová-Benková L. Evidence for the role of carboxyl groups in activity of endopolygalacturonase of *Aspergillus niger*. Chemical modification by carbodiimide reagent. Collect Czech Chem Commun. 1990;55:1389–95.
51. Rao MN; Kembhavi AA, Pant A. Implication of tryptophan and histidine in the active site of endo-polygalacturonase from *Aspergillus ustus*: elucidation of the reaction mechanism. Biochim Biophys Acta. 1996;1296:167–73.
52. Stratilová E, Dzúrová M, Markovic O, Jörnvall H. An essential tyrosine residue of Aspergillus polygalacturonase. FEBS Lett. 1996;382:164–6.

53. Lee DJ, Zeevaart JAD. Differential regulation of RNA levels of gibberellin dioxygenases by photoperiod in spinach. Plant physiol 2003;130:2085–94.
54. Bonner LJ, Dickinson HG. Anther dehiscence in *Lycopersicon esculentum* l. Structural aspects. New Phytol. 1989;113:97–115.
55. Keijzer CJ, Leferinkten Klooster HB, Reinders MC. The mechanics of the grass flower: anther dehiscence and pollen shedding in maize. Ann Bot.1996;78:15–21.
56. Garcia CC, Nepi M, Pacini E. Structural aspects and ecophysiology of anther opening in *Allium triquetrum*. Ann Bot. 2006;97:521–7.
57. Chichiricco G. Ripening and dehiscence of the anther in some Crocus (Iridaceae) species. Caryologia. 2000;53:255–60.
58. Cheng PC, Greyson RI, Walden DB. Comparison of anther development in genic-male-sterile and in male-fertile corn (*Zea mays*) from light microscopy and scanning microscopy. Can J Bot. 1979;57:578–96.
59. Bianchini M, Pacini L. Explosive anther dehiscence in *Ricinus communis* involves cell wall modifications and relative humidity. Int J Plant Sci. 1996;157:739–45.
60. Niu E, Shang X, Cheng C, Bao J, Zeng Y, Cai C, et al. Comprehensive analysis of the *COBRA-Like* (*COBL*) gene family in Gossypium identifies two *COBLs* potentially associated with fiber quality. PLoS One. 2015;10:e0145725.
61. Jung KW, Oh SI, Kim YY, Yoo KS, Cui MH, Shin JS. Arabidopsis histidine-containing phosphotransfer factor 4 (AHP4) negatively regulates secondary wall thickening of the anther endothecium during flowering. Mol Cells. 2008;25:294–300.
62. Gorguet B, Schipper D, van Lammeren A, Visser RG, van Heusden AW. *ps-2*, the gene responsible for functional sterility in tomato, due to non-dehiscent anthers, is the result of a mutation in a novel polygalacturonase gene. Theor Appl Genet 2009;118:1199–209.
63. Lyu M, Iftikhar J, Guo R, Wu B, Cao J. Patterns of expansion and expression divergence of the polygalacturonase gene family in *Brassica oleracea*. Int J Mol Sci. 2020;21:5706.
64. Keijzer C. The processes of anther dehiscence and pollen dispersal. I. The opening mechanism of longitudinally dehiscing anthers. New Phytol. 1987;105:487–9.
65. Plackett ARG, Thomas SG, Wilson ZA, Hedden P. Gibberellin control of stamen development: a fertile field. Trends Plant Sci. 2011;16:568–78.
66. Kobayashi M, Yamaguchi I, Murofushi N, Ota Y, Takahashi N. Fluctuation and localization of endogenous gibberellins in rice. J Agri Biol Chem. 1988;52.
67. Izhaki A, Borochov A, Zamski E, Weiss D. Gibberellin regulates post-microsporogenesis processes in petunia anthers. Physiol Plant. 2002;115:442–7.
68. Weiss D, Halevy AH. Stamens and gibberellin in the regulation of corolla pigmentation and growth in *Petunia hybrida*. Planta 1989;179:89–96.

69. Itoh H, Ueguchi-Tanaka M, Kawaide H, Chen X, Kamiya Y, Matsuoka M. The gene encoding tobacco gibberellin 3β-hydroxylase is expressed at the site of GA action during stem elongation and flower organ development. Plant J. 1999;20:15–24.
70. Itoh H, Ueguchi-Tanaka M, Sentoku N, Kitano H. Matsuoka M, Kobayashi M. Cloning and functional analysis of two gibberellin 3β-hydroxylase genes that are differently expressed during the growth of rice. Proc Natl Acad Sci USA 2001;98:8909–14.
71. Gocal GF, Sheldon CC, Gubler F, Moritz T, Bagnall DJ, MacMillan CP, et al. *GAMYB*-like genes, flowering, and gibberellin signaling in Arabidopsis. Plant Physiol. 2001;127:1682–93.
72. Tsuji H, Aya K, Ueguchi-Tanaka M, Shimada Y, Nakazono M, Watanabe R, et al. *GAMYB* controls different sets of genes and is differentially regulated by microRNA in aleurone cells and anthers. Plant J. 2006;47:427–44.
73. Radley ME. Effect of abscisic acid and gibberellic acid on grain set in wheat. Ann Appl Biol. 1980;95:409–14.
74. Colombo N, Favret EA. The effect of gibberellic acid on male fertility in bread wheat. Euphytica. 1996;91:297–303.
75. Millar AA, Gubler F. The Arabidopsis GAMYB-like genes, MYB33 and MYB65, are microRNA-regulated genes that redundantly facilitate anther development. Plant Cell. 2005;17:705–21.
76. Csukasi F, Donaire L, Casañal A, Martínez-Priego L, Botella MA, Medina-Escobar N. Two strawberry miR159 family members display developmental-specific expression patterns in the fruit receptacle and cooperatively regulate *Fa-GAMYB*. New Phytologist. 2012;195:47–57.
77. BioProject PRJNA285604. Sequencing and analysis of *Lupinus luteus*https://www.ncbi.nlm.nih.gov/bioproject/?term=PRJNA285604. Accessed 28 October 2020.
78. Schmittgen TD, Livak KJ. Analyzing real-time PCR data by the comparative C(T) method. Nat Protoc. 2008;3:1101–8.
79. FastPCR - an integrated tool for PCR primers design. http://primerdigital.com/fastpcr.html. Accessed 28 October 2020.
80. The Universal Probe Library Assay Design Center. https://lifescience.roche.com/en_pl/brands/universal-probe-library.html#assay-design-center. Accessed 28 October 2020.
81. Basic Local Alignment Search Tool. https://blast.ncbi.nlm.nih.gov/Blast.cgi. Accessed 28 October 2020.
82. The bioinformatics resource portal of the Swiss Institute of Bioinformatics. http://www.expasy.org/. Accessed 28 October 2020.
83. Translate tool. https://web.expasy.org/translate/. Accessed 28 October 2020.
84. ProtParam tool. https://web.expasy.org/protparam/. Accessed 28 October 2020.
85. Phylogenetic analysis pipeline by ETE3. https://www.genome.jp/tools/ete/. Accessed 28 October 2020.

86. Multiple Sequence Alignment by CLUSTALW. https://www.genome.jp/tools-bin/clustalw. Accessed 28 October 2020.
87. NCBI's Conserved Domain Database (CDD). (http://www.ncbi.nlm.nih.gov/Structure/cdd/wrpsb.cgi). Accessed 28 October 2020.
88. TMHMM Server for Prediction of transmembrane helices in proteins. http://www.cbs.dtu.dk/services/TMHMM/. Accessed 28 October 2020.
89. Phyre^2 - Protein Homology/analogy Recognition Engine. http://www.sbg.bio.ic.ac.uk/~phyre2/html/page.cgi?id=index. Accessed 28 October 2020.
90. DiAlign: Local multiple alignment. http://www.genomatix.de/cgi-bin/dialign/dialign.pl. Accessed 28 October 2020.
91. Robetta - protein structure prediction service. http://new.robetta.org/. Accessed 28 October 2020.
92. UCSF ChimeraX - visualization program from the Resource for Biocomputing, Visualization, and Informatics (RBVI). https://www.cgl.ucsf.edu/chimerax/. Accessed 28 October 2020.

Figures

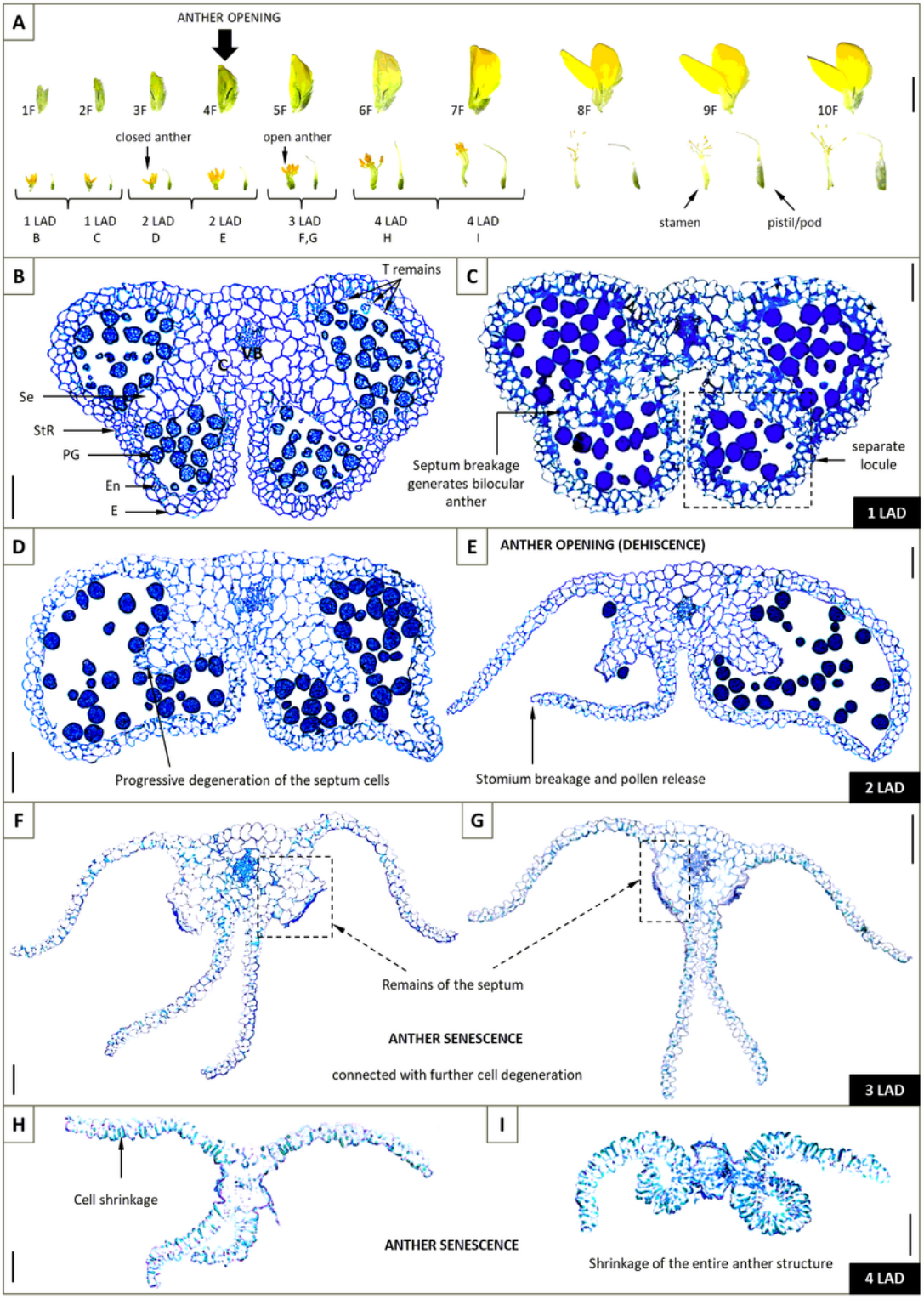

Figure 1

(A) Individual stages of flower (1F–10F) development in yellow lupine. After completing the dehiscence program (1F-3F), anther opening occurred about the fourth phase of flower development (4F) when flower and completely closed. Then follows pollination, fertilization, as well as pod setting and development (5F-10F). First and second stages of flower development correspond to first stage of late anther development (LAD); third and fourth stages of flower development relate to second stage of LAD; fifth stage of flower

development is parallel to third stage of LAD; sixth and seventh stages of flower development link to fourth stage of LAD. (B-I) The anatomical structure of yellow lupine anthers in different stages of late development. Cross-sections were stained with toluidine blue and anthers were photographed by light microscopy. C – connective, VB – vascular bundle, Se – septum, StR – stomium region, PG – pollen grain, En – endothecium, E – epidermis, T – tapetum. Scale bars = 1 cm (A); 50 μm (B-I).

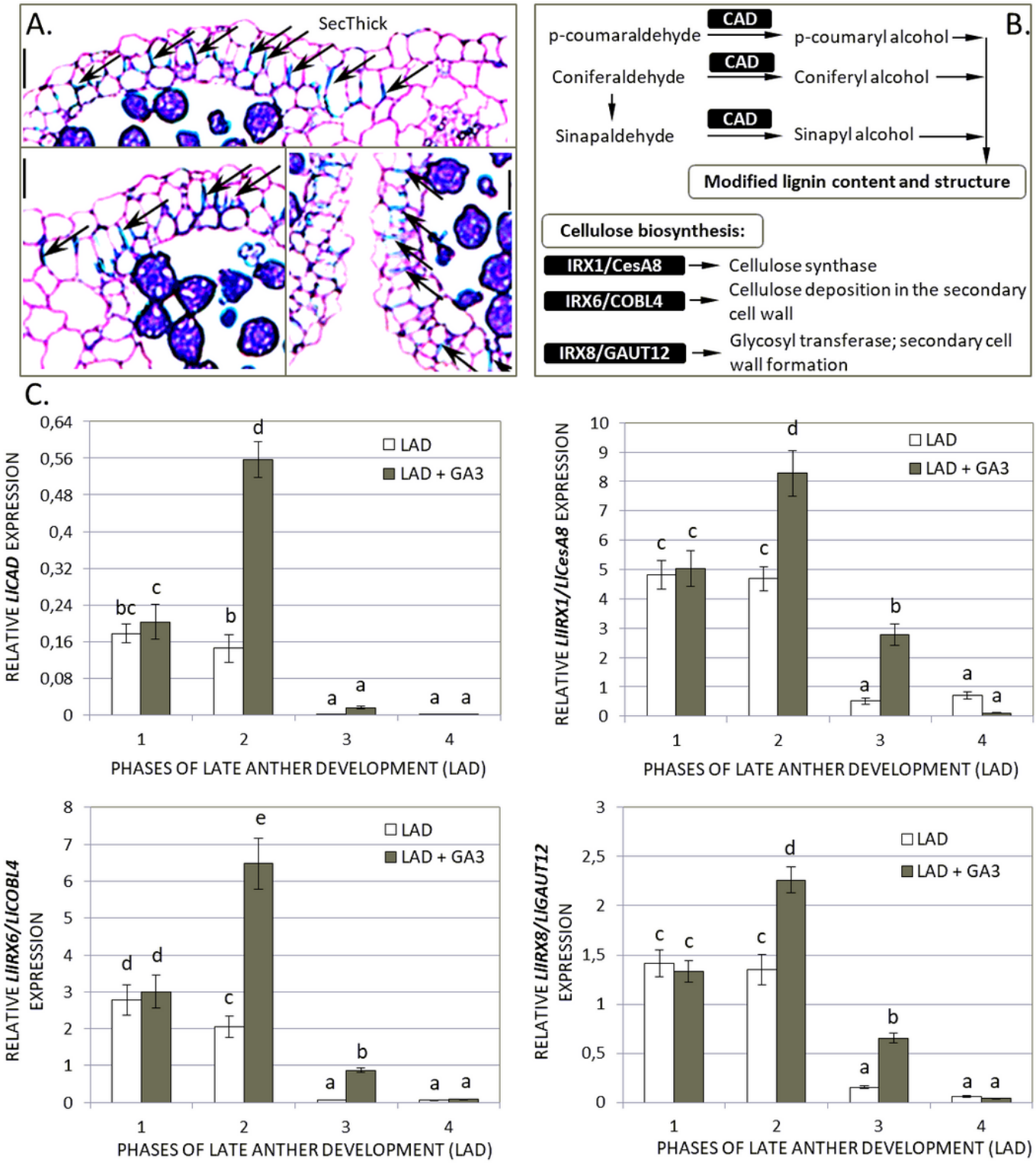

Figure 2

(A) Localization of secondary thickening (SecThick) within endothecial cell walls of yellow lupine anther. Transverse sections were stained with toluidine blue. Anthers were photographed by light microscopy; (B) The function of typical lignin (CAD, CINNAMYL ALCOHOL DEHYDROGENASE) and cellulose (IRX1/CesA8, IRREGULAR XYLEM1/Cellulose synthase A catalytic subunit 8; IRX6/COBL4, COBRA-like4; IRX8/GAUT12, GAlactUronosylTransferase12) biosynthesis-related genes [15, 18, 36, 37]; (C) Transcriptional activity of investigated genes (related to LIACT) during late anther development (LAD) and after gibberellic acid treatment (LAD + GA3, 100 µM). The average values of the three repetitions containing two replicates with standard errors (SE) were used to draw the figures. Letters represent statistically significant differences at $p < 0.05$ (one-way ANOVA followed by Tukey's Honest Significant Difference test). Scale bars = 25 µm.

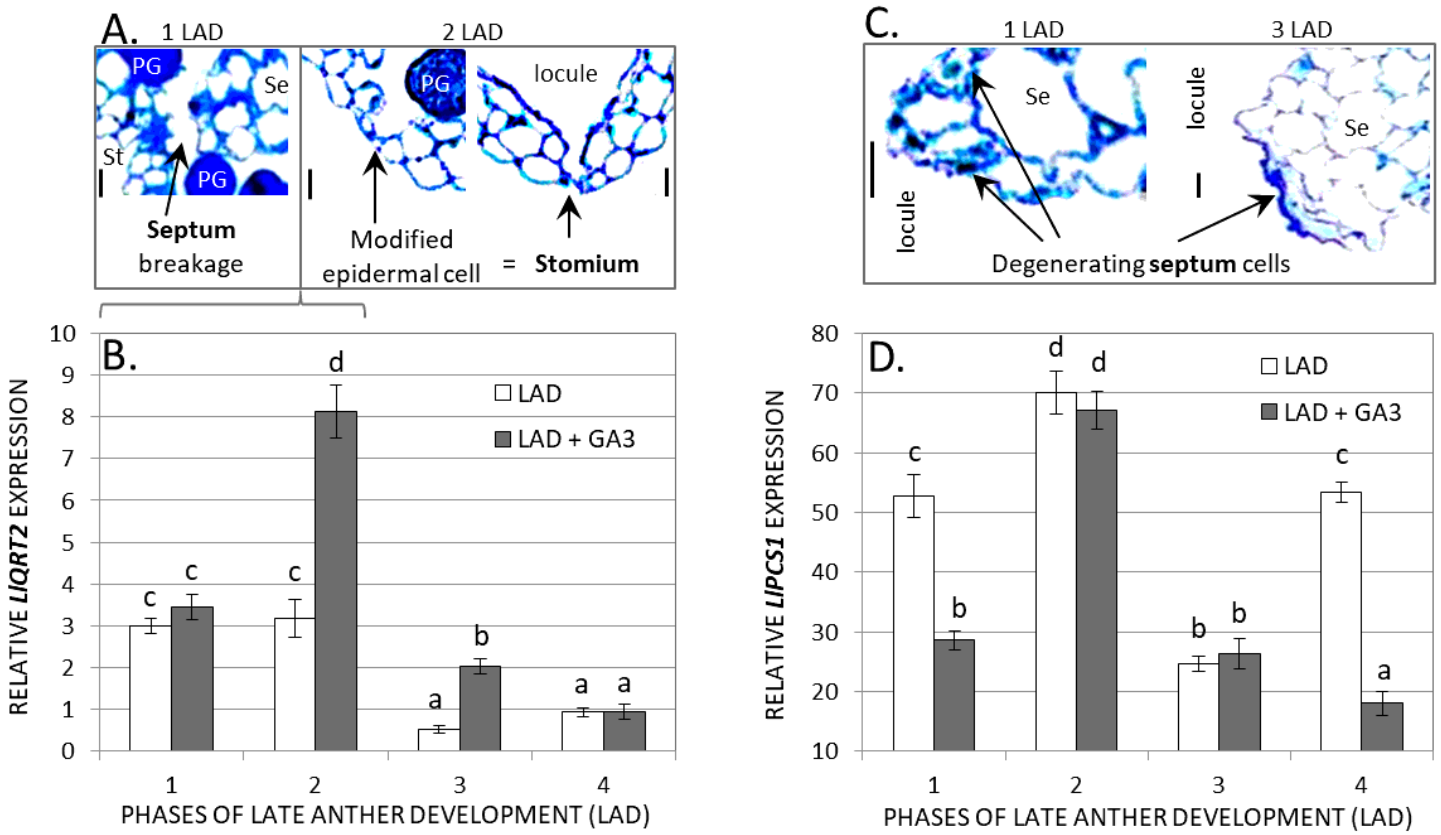

Figure 3

(A) Rupture of the septum (Se) and stomium (St) cells in the first and second late anther developmental (LAD) stages of yellow lupine; (C) Progressive degeneration of septum cells in first and third LAD stages. All transverse sections were stained with toluidine blue. Anthers were photographed by light microscopy; (B, D) Expression profile of LIQRT2 (QUARTET2) and LIPCS1 (PROMOTION OF CELL SURVIVAL1) in relation to the LIACT (ACTIN) during different stages of LAD, as well as after gibberellic acid GA3 application (LAD + GA3, 100 µM). PG – pollen grain. The average values of the three repetitions containing two replicates with standard errors (SE) were used to draw the figures. Letters represent statistically significant differences at $p < 0.05$ (one-way ANOVA followed by Tukey's HSD test). Scale bars = 10 µM.

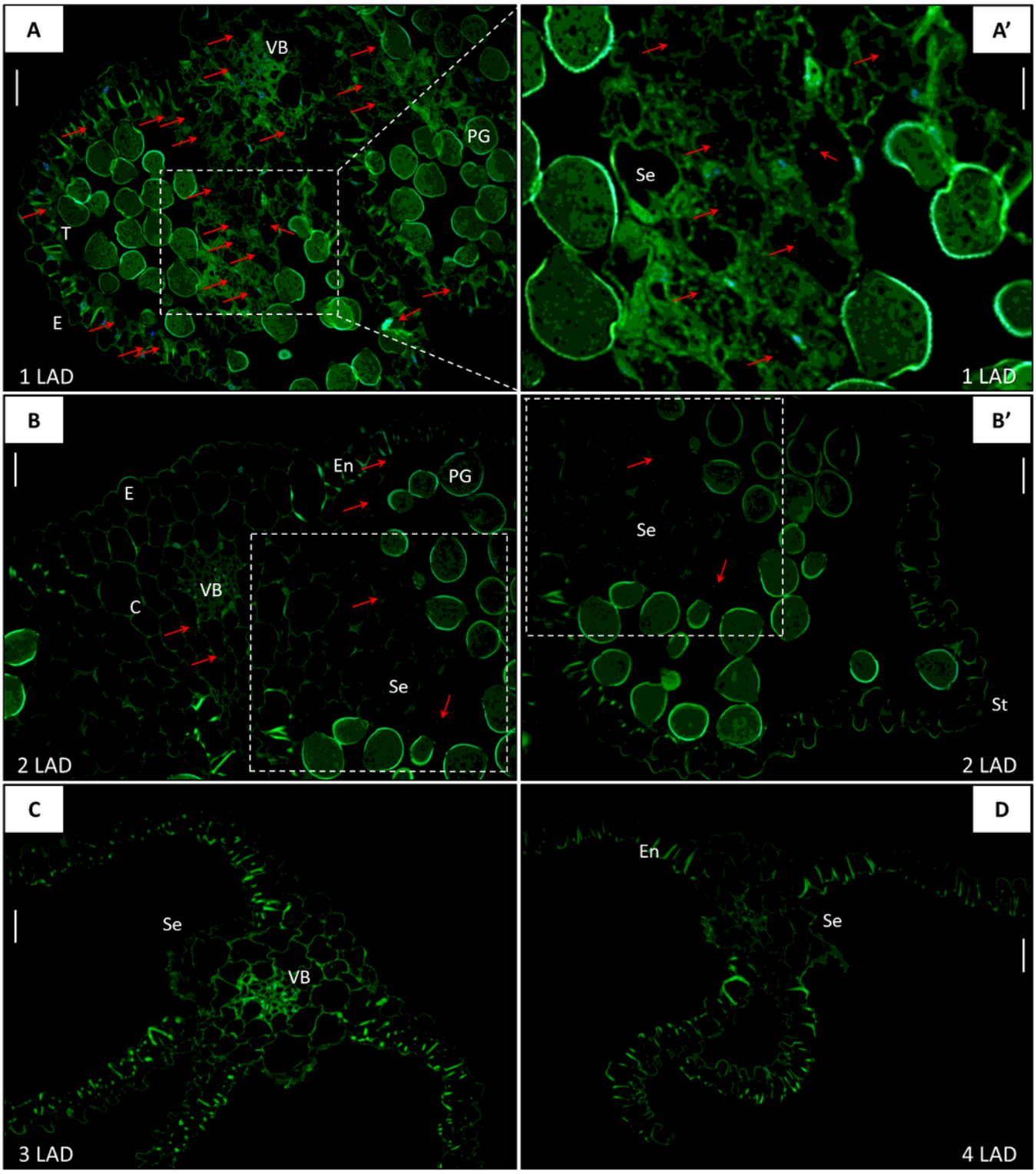

Figure 4

Gibberellic acid (GA3) immunolocalization in all selected stages (1-4) of late anther development (LAD) in yellow lupine. Green fluorescence corresponds to GA3 accumulation, while blue fluorescence indicates cell nuclei stained with DAPI. The red arrows indicate GA3 signal. The subfigure A' is an enlargement of subfigure A. The square marked with the dashed line in subfigures B and B' indicates the same area of cells. The autofluorescence of the cell walls and pollen grains is visible. VB – vascular bundle, PG - pollen

grain, E - epidermis, En - endothecium, T - tapetum, C - connective, Se – septum, St - stomium. Scale bars: 25 µm (A, B, B', C, D), 10 µm (A').

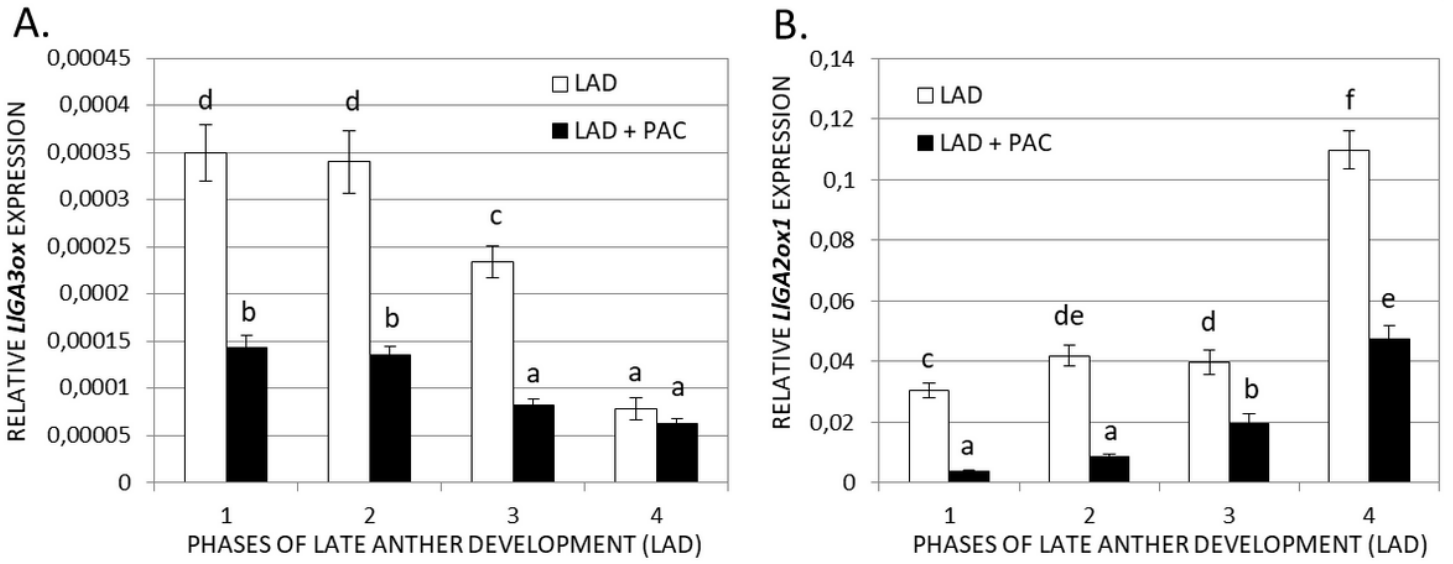

Figure 5

The relative transcript levels of LIGA3ox (Gibberellin 3-oxidase) connected with GA biosynthesis (A), and LIGA2ox1 (Gibberellin 2-oxidase 1) involved in GA deactivation (B) were investigated during late anther development (LAD) of yellow lupine. Some anthers were treated with solution of paclobutrazol (LAD + PAC, 100 µM) in 0.05% Tween 20, while some with only 0.05% Tween 20 (LAD). LIACT (ACTIN) was used as an internal control. Values are presented as the mean of three biological and two technical replicates. Error bars indicate SEs. Letters represent significant differences at $p < 0.05$ (one-way ANOVA followed by Tukey's HSD test).

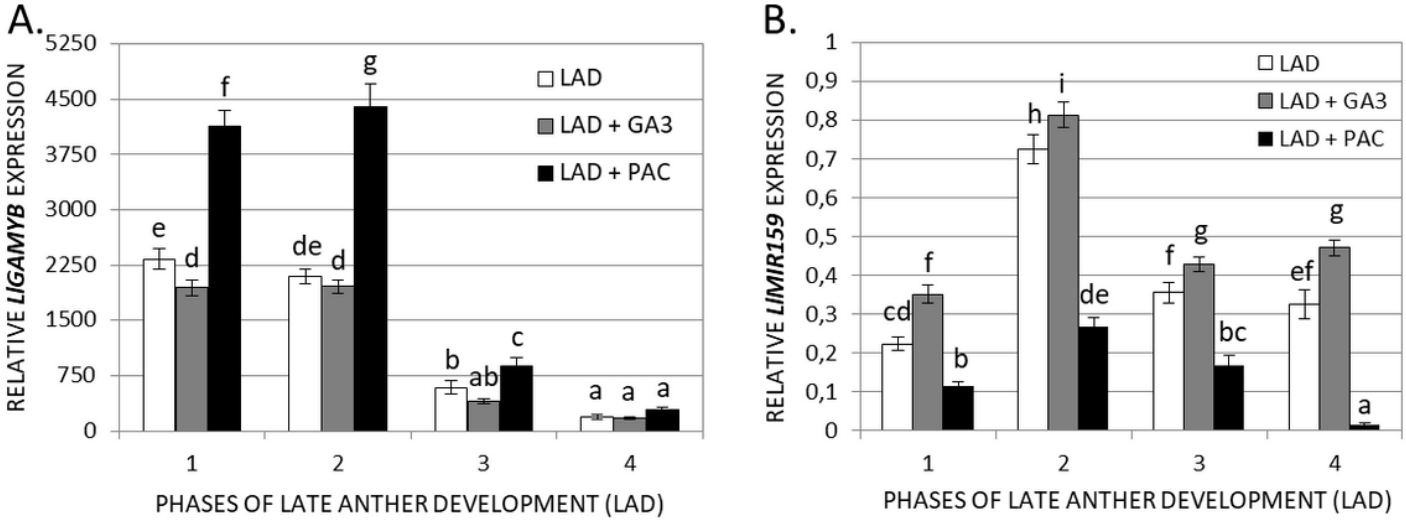

Figure 6

Relative transcriptional activity of LIGAMYB involved in GA signaling (A) and LIMIR159 associated with cutting GAMYB transcripts during late anther development (LAD) of yellow lupine. Some anthers were treated with solution of GA3 (LAD + GA3, 100 μM) in 0.05% Tween 20, some with solution of paclobutrazol (LAD + PAC, 100 μM) in 0.05% Tween 20, while some with only 0.05% Tween 20 (LAD). LIACT (ACTIN) was used as an internal control. Values are presented as the mean of three biological and two technical replicates. Error bars indicate SEs. Letters represent statistically significant differences at $p < 0.05$ (one-way ANOVA followed by Tukey's HSD test).

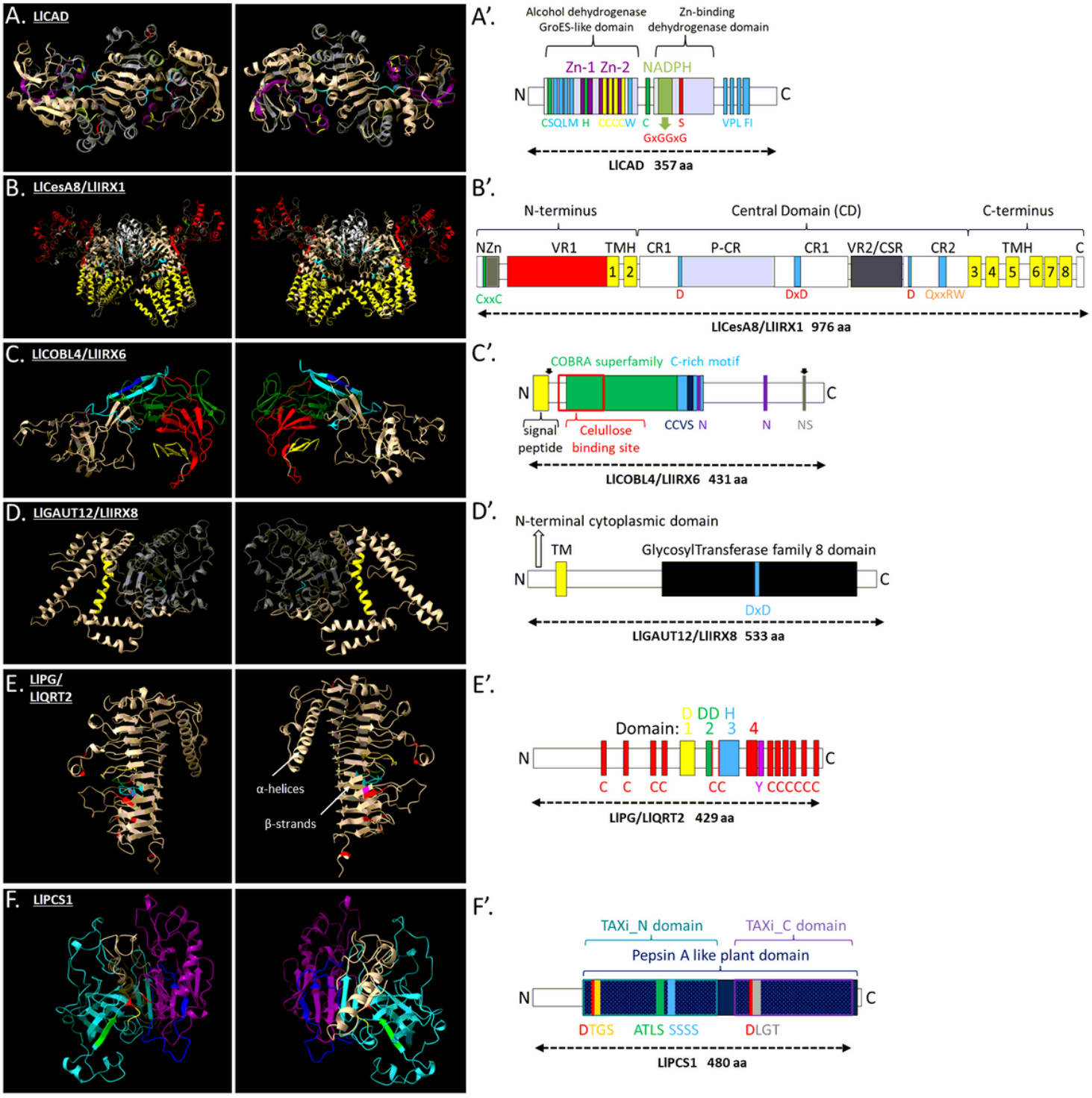

Figure 7

The domain structures of LlCAD (Cinnamyl Alcohol Dehydrogenase); LlCesA8/LlIRX1 (Cellulose synthase A catalytic subunit 8/IRREGULAR XYLEM1); LlCOBL4/IRX6 (COBRA-like4); LlGAUT12/LlIRX8 (GAlactUronosylTransferase12); LlPG/LlQRT2 (Polygalacturonase/ QUARTET2) and LlPCS1 (PROMOTION OF CELL SURVIVAL1) identified in yellow lupine (Lupinus luteus L.). (A-F) The predicted tertiary 3D models constructed by ROBETTA protein modeling server visualized by the ChimeraX program; (A'-F') Conserved domains, motifs and specific amino acids identified via different tools described in method section. The colors used in the 3D protein models correspond to the colors presented in the protein diagrams. The specific functions of domains/motifs/amino acids are described in details in table 1.

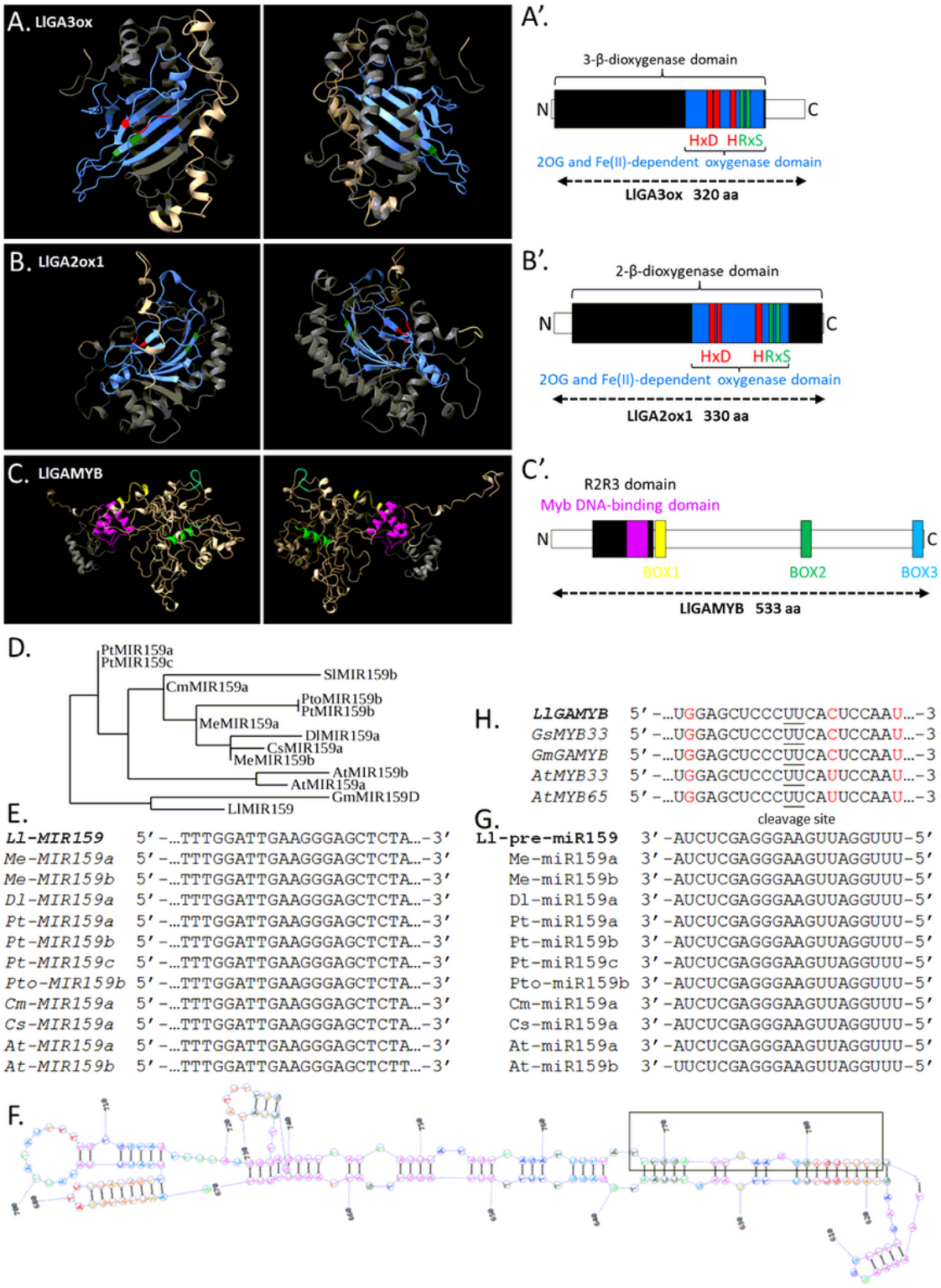

Figure 8

The domain structures of LlGA3ox (Gibberellin 3-oxidase); LlGA2ox1 (Gibberellin 2-oxidase1) and LlGAMYB identified in yellow lupine (Lupinus luteus L.); (A-C) The predicted tertiary 3D models constructed by ROBETTA protein modeling server visualized by the ChimeraX program; (A'-C') Conserved domains, motifs and specific amino acids identified via different tools described in method section. The colors used in the 3D protein models correspond to the colors presented in the protein diagrams. The

specific functions of domains/motifs/amino acids are described in details in table 1; (D-H) Analysis of Ll-pre-miR159 sequence identified in yellow lupine; (D) The phylogenetic relationship of the Ll-MIR159 compared with MIR159 from various plant species; (E) Alignment of part of nucleotide sequence (21 bp which form a mature miRNA) of Ll-MIR159 with closely related fragments of MIR159 from other plant species; (F) Secondary stem-loop structure of the Ll-pre-miR159 and localization of mature miR159 on the stem of the precursor sequence (marked with a rectangle); (G) Alignment of the nucleotide sequences of Ll-pre-miR159 with a mature miR159 from different plant species; (H) The LlGAMYB mRNA cleavage site is designated between 11th and 12th base from the 5' end (underlined), and comparison to other plant species. Red letters represent mis-matches between GAMYB sequences and miR159s; Ll – Lupinus luteus (MW240683, Ll-MIR159; MW240675, LlGAMYB), Me – Manihot esculenta (JX013999, JX014000), Dl – Dimocarpus longan (MT920321), Pt – Populus trichocarpa (AY728394, AY728395, AY728401), Pto – Populus tomentosa (MF463031), Cm – Cucumis melo (NR_120776), Cs – Citrus sinensis (NR_129302), At – Arabidopsis thaliana (NR_139941/At-miR159a, NR_139756/At-miR159b, AAS10086/AtMYB33, AAS10055/AtMYB65), Gs - Glycine soja (XP_028187659), Gm – Glycine max (AHB19229).

Supplementary Files

This is a list of supplementary files associated with this preprint. Click to download.

- SupMat2.pptx
- Supplementarymaterials21.12.20.pptx